 Related Commentary, page 516

# Human tumors instigate granulin-expressing hematopoietic cells that promote malignancy by activating stromal fibroblasts in mice

Moshe Elkabets,[1] Ann M. Gifford,[2] Christina Scheel,[2] Bjorn Nilsson,[1,3] Ferenc Reinhardt,[2] Mark-Anthony Bray,[3] Anne E. Carpenter,[3] Karin Jirström,[4] Kristina Magnusson,[5] Benjamin L. Ebert,[1,3] Fredrik Pontén,[5] Robert A. Weinberg,[2,6,7] and Sandra S. McAllister[1]

[1]Department of Medicine, Hematology Division, Brigham and Women's Hospital, Harvard Medical School, Boston, Massachusetts, USA. [2]Whitehead Institute for Biomedical Research, Cambridge, Massachusetts, USA. [3]Broad Institute of MIT and Harvard, Cambridge, Massachusetts, USA. [4]Center for Molecular Pathology, Department of Laboratory Medicine, Lund University, Malmö University Hospital, Malmö, Sweden. [5]Department of Genetics and Pathology, Rudbeck Laboratory, Uppsala University, Uppsala, Sweden. [6]Department of Biology, Massachusetts Institute of Technology, Cambridge, Massachusetts, USA. [7]MIT Ludwig Center for Molecular Oncology, Cambridge, Massachusetts, USA.

**Systemic instigation is a process by which endocrine signals sent from certain tumors (instigators) stimulate BM cells (BMCs), which are mobilized into the circulation and subsequently foster the growth of otherwise indolent carcinoma cells (responders) residing at distant anatomical sites. The identity of the BMCs and their specific contribution or contributions to responder tumor growth have been elusive. Here, we have demonstrated that Sca1$^+$cKit$^-$ hematopoietic BMCs of mouse hosts bearing instigating tumors promote the growth of responding tumors that form with a myofibroblast-rich, desmoplastic stroma. Such stroma is almost always observed in malignant human adenocarcinomas and is an indicator of poor prognosis. We then identified granulin (*GRN*) as the most upregulated gene in instigating Sca1$^+$cKit$^-$ BMCs relative to counterpart control cells. The GRN$^+$ BMCs that were recruited to the responding tumors induced resident tissue fibroblasts to express genes that promoted malignant tumor progression; indeed, treatment with recombinant GRN alone was sufficient to promote desmoplastic responding tumor growth. Further, analysis of tumor tissues from a cohort of breast cancer patients revealed that high GRN expression correlated with the most aggressive triple-negative, basal-like tumor subtype and reduced patient survival. Our data suggest that GRN and the unique hematopoietic BMCs that produce it might serve as novel therapeutic targets.**

## Introduction

Patients diagnosed with 1 malignant neoplasm are at a greatly increased risk of presenting with multiple, independent primary cancers within a relatively short time period after the initial diagnosis (1, 2). As an example, some breast cancer patients develop contralateral breast cancer, which is a predictor of poor outcome (3, 4), and patients with synchronous bilateral breast cancer tend to have a significantly worse overall survival than those patients with metachronous or unilateral cancers (5). In addition to secondary tumors, patients with recurrent disease often present with multiple metastases that appear to arise suddenly and synchronously. As was recently reported, surgical resection of primary breast cancers significantly improved the survival time of patients who presented with distant metastases at the time of their primary diagnosis (6, 7). While there are a number of possible explanations for these diverse clinical observations, experimental evidence demonstrates that certain tumors can affect the behavior of other tumor(s) residing at distant anatomical sites (reviewed in ref. 8). The mechanisms underlying these systemic interactions between multiple dispersed tumors within a host are poorly understood.

In our own work, we reported that certain tumors can foster the growth of other tumors or disseminated metastatic cells located at distant anatomical sites in host animals (9). These studies revealed that certain tumor cells that would otherwise remain indolent are capable of responding to systemic cues to become overt tumors (9). Thus, when we implanted vigorously growing human breast carcinomas cells (which we termed *instigators*) in host mice, they stimulated both the outgrowth of otherwise poorly tumorigenic, indolent transformed cells (which we termed *responders*) residing at contralateral sites as well as the colonization of otherwise weakly metastatic cells residing in the lungs. We termed this endocrine stimulation *systemic instigation*. Importantly, instigated responding tumors were formed exclusively from the implanted responder cells and were therefore not seeded by metastatic cells originating in the instigating tumor (9).

A number of reports have demonstrated that tumors employ various means to actively perturb host organs at distant anatomical sites and that these perturbations are a driving force in tumor progression (reviewed in ref. 8). In our own experiments, we showed that instigating tumors perturb the BM of the tumor-bearing host by activating BM cells (BMCs) via a process that depended on secretion of osteopontin (OPN) by instigating tumor cells. Thus, when we mixed the indolent responder cells directly with BMCs from instigating tumor-bearing hosts prior to implantation, the admixed BMCs were able to instigate the growth of the otherwise indolent responder cells; admixed BMCs from control mice that did not bear an instigating tumor failed to do so (9).

**Authorship note:** Moshe Elkabets and Ann M. Gifford, as well as Robert A. Weinberg and Sandra S. McAllister, contributed equally to this work.

**Conflict of interest:** The authors have declared that no conflict of interest exists.

**Citation for this article:** *J Clin Invest.* 2011;121(2):784–799. doi:10.1172/JCI43757.

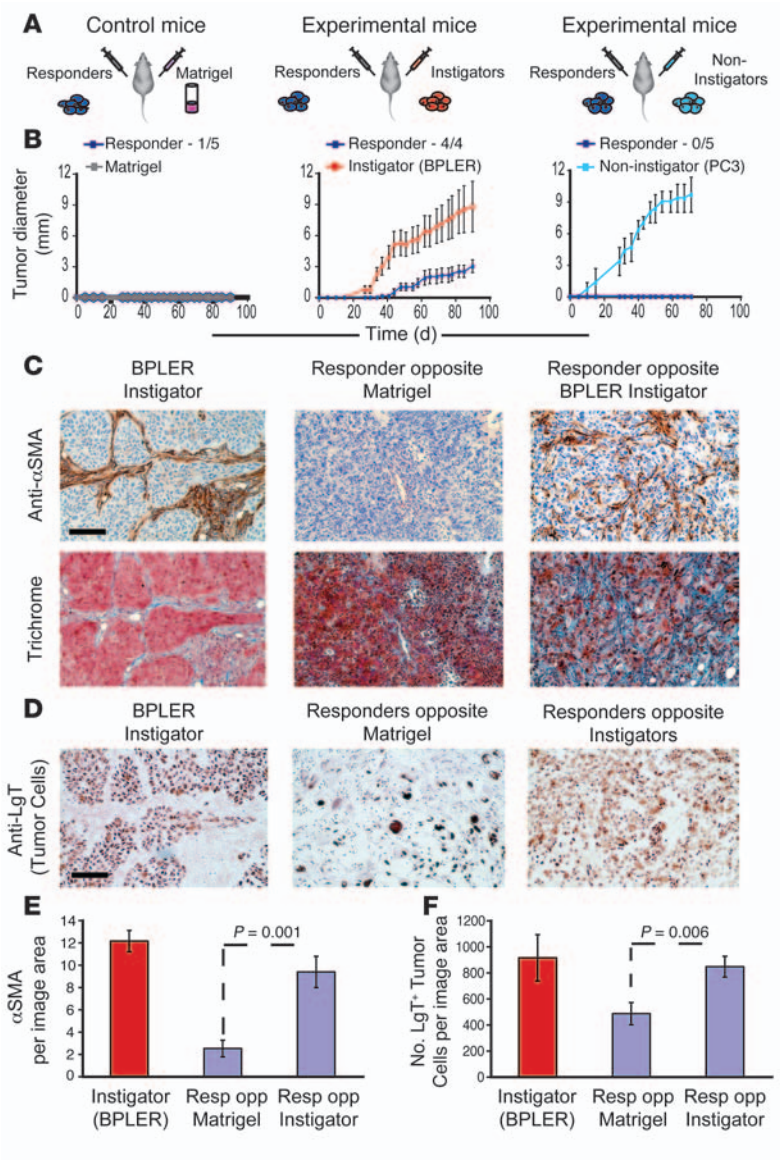


**Figure 1**
Systemic instigation of responding tumor growth and stromal desmoplasia. (**A**) Systemic instigation injection scheme. HMLER-HR transformed cells (responders) are injected subcutaneously into 1 flank of host mice. The opposite flank is injected with either a Matrigel control or aggressively growing tumor cell lines (instigators or noninstigators). (**B**) Growth kinetics of instigating and responding tumors. Of the responder cell injections, 1 of 5 formed tumors opposite Matrigel, 4 of 4 formed growing tumors opposite instigating BPLER tumors, and 0 of 5 formed tumors opposite noninstigating PC3 tumors. (**C**) Histopathology of resulting BPLER and HMLER-HR tumors 90 days after injection. Top panel shows αSMA staining of myofibroblasts and pericytes (brown) and hematoxylin counterstaining of nuclei (blue). Bottom panel shows Masson's trichrome staining for collagen (blue) and nuclei counterstaining (dark pink). Scale bar: 100 μm. (**D**) Staining for the SV40 LgT (brown) to identify tumor cells in the resulting tumor tissues. Scale bar: 100 μm. (**E** and **F**) CellProfiler quantification of area occupied by αSMA$^+$ staining (**E**) and number of LgT$^+$ cells (**F**) in images of resulting tumor tissues under indicated conditions. An average of 10 images of instigating tumors and the contralateral responding tumors (Resp opp instigator) and 5 images of the responding tumor recovered opposite Matrigel (Resp opp Matrigel) were used for quantification. Data are expressed as mean ± SEM.

Under situations of systemic instigation, such activated BMCs apparently became mobilized into the circulation, after which they were recruited into the stroma of the distant, otherwise indolent responding tumors. These observations, as well as those of others, have demonstrated that certain types of BMCs are functionally activated even prior to their mobilization into the circulation and subsequent recruitment to both primary tumors and distant indolent metastases (9, 10).

These clinical and experimental observations highlighted the need for a better understanding of the systemic mechanisms that operate to induce growth of tumors that would otherwise remain indolent. Thus, our previous studies did not reveal the identity of the activated BMC subpopulation or subpopulations that represent the key intermediaries between the instigating and responding tumors. Furthermore, other than promoting their growth, the precise benefits that the instigator-activated BMCs confer on responding tumors have been elusive. Accordingly, we undertook studies to deepen our understanding of the endocrine instigation process and to identify the mechanisms by which BMCs that are activated by instigating tumors are able to facilitate the outgrowth of responding tumors.

## Results

*Histopathology of responding tumors that arise as a consequence of systemic instigation.* To begin to elucidate the mechanisms by which responding tumor growth is instigated, we chose to examine the histopathology of instigated responding tumors. To do so, we injected either BPLER (11) or MDA-MB-231 human breast cancer cells as instigators subcutaneously into one flank of Nude mice and weakly tumorigenic, transformed mammary epithelial HMLER-HR cells (12) as responders into the contralateral flanks of these mice (Figure 1A). In control groups of mice, we injected either noninstigating tumor cells (PC3) or Matrigel vehicle contralaterally to the indolent responder cells (Figure 1A). Consistent with our previously reported results, the responding cells formed rapidly growing tumors only in the presence of the contralateral instigating tumors (Figure 1B and Supplemental Figure 1A; supplemental material available online with this article; doi:10.1172/JCI43757DS1) without any evidence of being seeded by disseminated instigator cells (9).

Striking differences were observed when we compared the histopathology of the responding tumors that had grown opposite instigating tumors with the few, small control responding masses

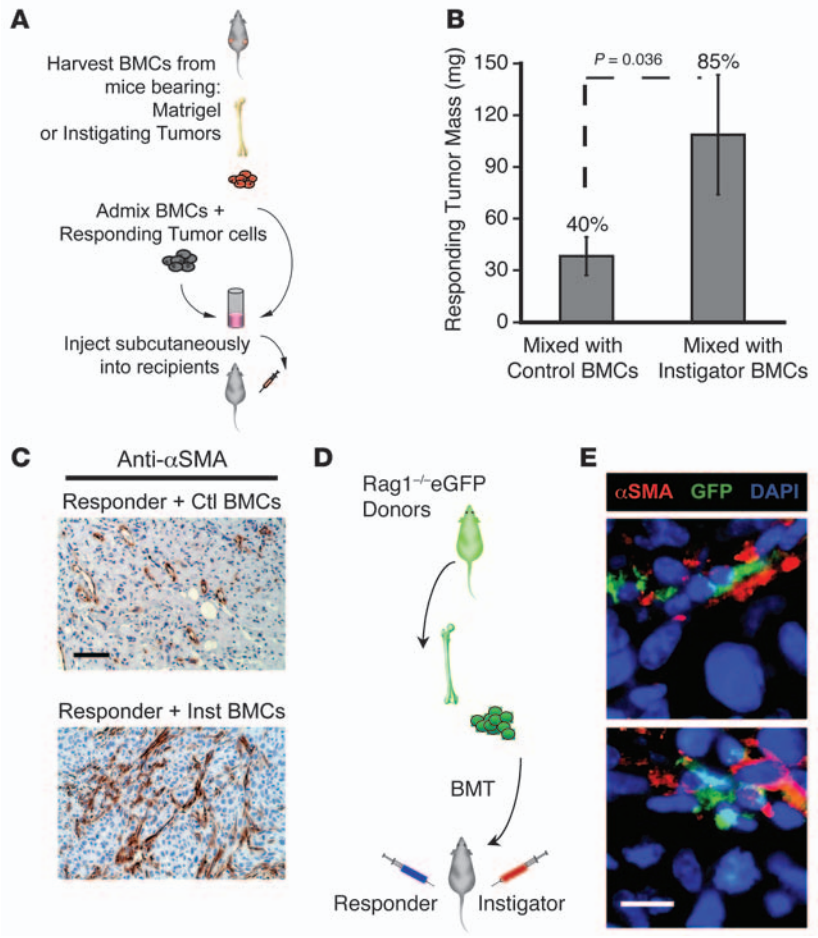


**Figure 2**
BMCs from instigator-bearing animals phenocopy systemic instigation. (**A**) Experimental scheme to test BMC tumor supportive function: admixtures of BMCs and responding tumor cells are injected subcutaneously into host nude mice. (**B**) Average mass of resulting tumors 12 weeks after implantation of various indicated mixtures. Tumor incidence is indicated above bars (2 separate experiments, $n$ = 16 per group). Data are expressed as mean ± SEM. (**C**) Histopathology of resulting responding tumors harvested 12 weeks after implantation of indicated mixtures. Photomicrographs show staining for αSMA (brown) and nuclei counterstained with hematoxylin (blue). Scale bar: 100 μm. (**D**) Experimental scheme for injecting tumor cells subcutaneously into mice that had previously been engrafted with GFP$^+$ BMCs. (**E**) Merged immunofluorescent images of responding tumors that had grown for 12 weeks opposite BPLER (top) or MDA-MB-231 (bottom) instigating tumors in GFP$^+$ BMC transplanted mice. Images represent GFP$^+$ BM–derived cells (green); αSMA$^+$ tumor myofibroblasts and pericytes (red); and cell nuclei (DAPI; blue). Yellow signal represents an overlap of 2 different cells, as confirmed by confocal microscopy. Scale bar: 25 μm.

that eventually appeared. In particular, we examined these various tumors for the presence of αSMA-positive myofibroblasts and collagen deposition, both of which are hallmarks of a reactive, desmoplastic stroma (13).

Responding cell masses recovered from sites contralateral to Matrigel plugs displayed very little collagen deposition or αSMA expression (Figure 1C). In fact, the few αSMA-positive cells that we did observe within these growths also expressed the pericyte marker NG2 and were associated with expression of the mouse endothelial cell antigen MECA32 (data not shown). These findings indicated that the αSMA-positive cells present in these masses were capillary-associated pericytes rather than myofibroblasts (14, 15).

In striking contrast, αSMA-positive cells and collagen were distributed widely and uniformly throughout the responding tumors that had been implanted contralaterally to either BPLER or MDA-MB-231 instigating tumors (Figure 1C and Supplemental Figure 1B). Staining for αSMA in these responding tumors overlapped only to a minimal extent with the staining for NG2 and MECA32 (Supplemental Figure 1C and data not shown), indicating that the majority of αSMA$^+$ cells in these instigated tumors were myofibroblasts rather than capillary-associated pericytes. Such myofibroblast-rich, reactive stroma is almost always observed in malignant human adenocarcinomas and is associated with invasiveness and poor prognosis (16, 17). We also noted features of stromal desmoplasia, though not as well developed, in the lung metastases that formed in the presence of subcutaneously implanted instigating tumors (Supplemental Figure 2).

CellProfiler image analysis (18, 19) revealed that the area covered by αSMA-positive cells was 3-fold higher in the instigated tumors than that in the control tumors ($P$ = 0.001; Figure 1E). In fact, these levels of αSMA staining approached those observed in the contralateral instigating tumors (Figure 1, C and E). We could not include analysis of responding tumors residing opposite noninstigators, as no responding tumors formed under these circumstances. We also calculated the average number of responding tumor cells, as determined by positive staining for the large T antigen (LgT) (Figure 1D and Supplemental Figure 1B). We determined that the numbers of responding tumor cells within these masses were significantly higher in the instigated tumor masses than in controls ($P$ = 0.006; Figure 1F).

Hence, the increase in tumor mass that we observed as a consequence of systemic instigation was due to expansion of both the epithelial and stromal compartments within the instigated tumor tissues. Moreover, recruitment of myofibroblasts into responding tumors was initiated on a systemic level, regardless of the sites where responding tumors resided.

*Influence of activated BM cells on responding tumor histopathology.* One previously noted consequence of systemic instigation is the enhanced recruitment of BM-derived cells into the responding tumor stroma (9). Moreover, BMCs extracted from instigator-bearing mice, when mixed directly with responding tumor cells, could

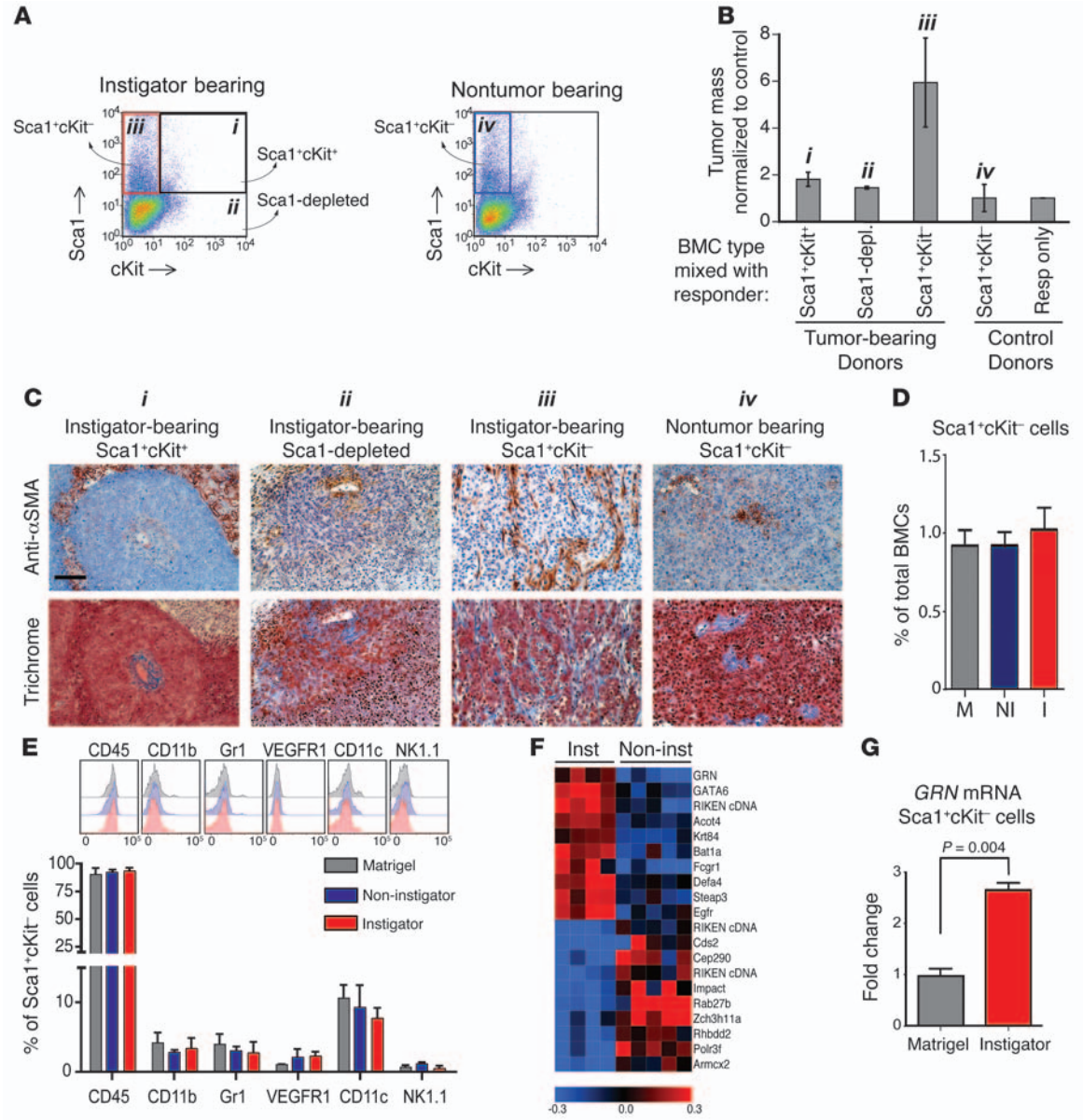


**Figure 3**

Sca1+cKit− hematopoietic BMCs are activated by instigating tumors. (**A**) FACS density plots representing the collection of the following BMC populations from instigating tumor-bearing mice: Sca1+cKit+ (population i), Sca1 depleted (population ii), and Sca1+cKit− (population iii). BMC population collected from control mice: Sca1+cKit− (population iv). (**B**) Relative average mass of resulting tumors 12 weeks after subcutaneous injection of responder-BMC mixtures. Tumor mass was normalized to the mass of control responder tumors that had grown on their own (3 separate experiments; $n = 18$ per group). (**C**) Histopathology of responding tumors resulting from the indicated admixtures. Top panel shows αSMA staining of myofibroblasts and pericytes (brown) and hematoxylin counterstaining of nuclei (blue). Bottom panel shows Masson's trichrome staining for collagen (blue) and cell nuclei (dark pink). Scale bar: 100 μm. (**D**) Representation of Sca1+cKit− BMCs as percentage of total BMCs from mice bearing Matrigel plugs (gray), noninstigating tumors (blue), or instigating tumors (red). (**E**) Flow cytometric analysis of Sca1+cKit− BMCs from mice bearing Matrigel plugs (gray), noninstigating tumors (blue), or instigating tumors (red). Histograms represent staining intensity for indicating cell-surface antigen markers. Graph represents average percentage of Sca1+cKit− cells that were positive for the indicated cell-surface antigens ($n = 4$ per group). No significant differences were observed between groups. (**F**) Partial heat map showing differential gene expression analysis of Sca1+cKit− BMCs from instigator-bearing mice (BPLER, $n = 4$) compared with those from size-matched noninstigator-bearing mice (PC3, $n = 5$). (**G**) Fold change of *GRN* mRNA expression (qPCR) in sorted Sca1+cKit− BMCs prepared from indicated mice ($n = 4$ per group). Data are expressed as mean ± SEM.

stimulate the growth of responding tumors and thereby mimic the effects of systemic instigation (9). This response provided us with a functional test of the biological status of the BM, more specifically, of the ability of its component cells to expedite indolent tumor growth. We exploited this test to determine whether the stromal desmoplasia observed in the responding tumors implanted opposite instigating tumors was phenocopied by the admixed BMCs prepared from instigator-bearing animals.

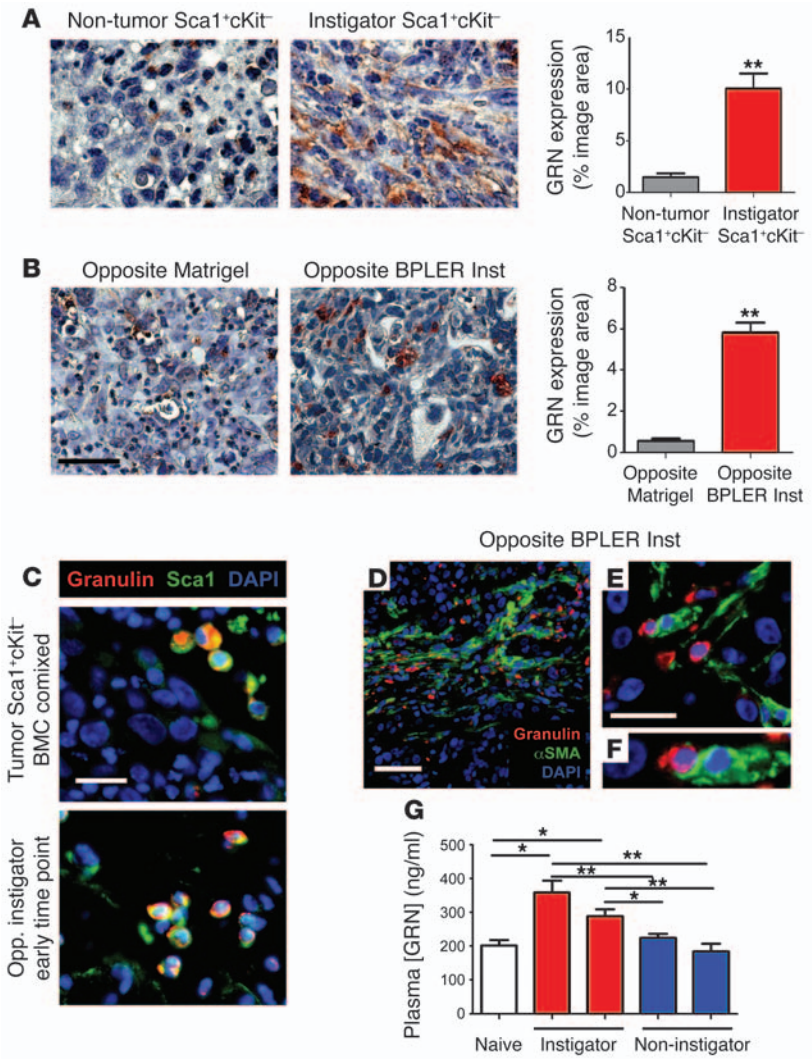


**Figure 4**

GRN+ BMCs are selectively recruited to instigated tumors but do not give rise directly to tumor myofibroblasts. (**A**) Representative immunohistochemical staining of responding tumors 14 weeks after injecting admixtures of responder cells with Sca1+cKit– BMCs from control (left) or instigator-bearing mice (right). Tissues were stained for GRN (red) and nuclei were counterstained with hematoxylin (blue). Original magnification, ×630. Graph represents CellProfiler quantification of image area covered by positive GRN staining of indicated responding tumors ($n = 3$ images per group; $P < 0.01$). (**B**) Representative immunohistochemical staining of responding tumors 12 weeks after injecting responder cells contralaterally to either control (left) or instigating tumor cells (right). Images show GRN staining (red) and nuclei counterstaining with hematoxylin (blue). Scale bar: 50 μm. Graph represents CellProfiler quantification of image area covered by positive GRN staining of indicated responding tumors ($n = 5$ images per group; $P < 0.01$). (**C**) Top: merged immunofluorescent image representative of responding tumors at 14 weeks following admixture with Sca1+cKit– BMCs from instigator-bearing mice. Bottom: merged immunofluorescent image representative of responding tumors that had grown for 4 weeks contralaterally to BPLER instigating tumors. Tumors were stained for Sca1 (green) and GRN (red) and nuclei stained with DAPI (blue). Yellow indicates that Sca1+ cells also express GRN. Scale bar: 25 μm. (**D**–**F**) Merged immunofluorescent images of responding tumors that had grown for 12 weeks contralaterally to BPLER instigating tumors. Tumors were stained for GRN (red) and αSMA (green); nuclei were stained with DAPI (blue). Scale bars: 100 μm (**D**); 25 μm (**E**). **F** is a magnification of cells shown in **E**. (**G**) Graph representing concentration of GRN in plasma from instigator-bearing mice (red), noninstigator-bearing mice (blue), and tumor-free mice (white) ($n = 3$–5 per group; $^{**}P < 0.01$, $^{*}P < 0.05$). Data are expressed as mean ± SEM.

Thus, we mixed responding tumor cells with BMCs prepared from mice bearing either Matrigel plugs or BPLER instigating tumors prior to implantation (Figure 2A). In consonance with our previous work, admixture of BMCs from instigator-bearing animals increased the incidence of tumor formation from approximately 40% to 85% and enhanced the size of those tumors that did form by a factor of approximately 3 relative to tumors to which control BMCs had been admixed (Figure 2B).

We found that the admixed BMCs, like contralaterally implanted instigating tumors, influenced the histopathology of the responding tumors. Thus, when control BMCs from Matrigel-bearing mice were mixed with the responder cells, the resulting growths were devoid of desmoplastic stroma (Figure 2C). In these small masses, αSMA+ cells were restricted to blood vessels, indicating that they were capillary-associated pericytes (data not shown). In marked contrast, αSMA+ cells and collagen were abundant and distributed uniformly throughout the stroma of responding tumors resulting from the mixture of the responder cells with BMCs from instigator-bearing mice (Figure 2C and not shown); in these tumors, αSMA stained not only pericytes but also the myofibroblasts (Supplemental Figure 3). Hence, the reactive tumor stroma resulting from admixture of BMCs from instigator-bearing mice closely phenocopied the stroma of responding tumors implanted opposite instigating tumors.

*BMCs do not differentiate into responding tumor myofibroblasts*. Fibroblasts and myofibroblasts are known to confer a variety of physiologic benefits on tumors (20, 21). Thus, our observations suggested that the mechanism by which responding tumor growth was instigated depended on their ability to recruit myofibroblast-rich tumor-supportive stroma.

These initial observations did not reveal the mechanistic connection(s) between tumor growth and the formation of a reactive stroma, nor did they reveal whether the activated BMCs present in instigator-bearing mice contain progenitors of the stromal myofibroblasts. Reported observations vary on this point; some reports indicate that tumor myofibroblasts have origins in the BM and/or circulation, while others suggest that the nearby normal tissue of the host serves as the immediate source of tumor myofibroblasts (22–24).

To resolve between these alternatives, we examined the responding tumors that arose as a result of systemic instigation in host mice that had previously received BM transplants from donor mice expressing GFP (*Rag1*$^{-/-}$*eGFPTg* mice; ref. 9) (Figure 2D). While GFP+ BM–derived cells were indeed incorporated into the stroma of instigated responding tumors that had formed in the recipient

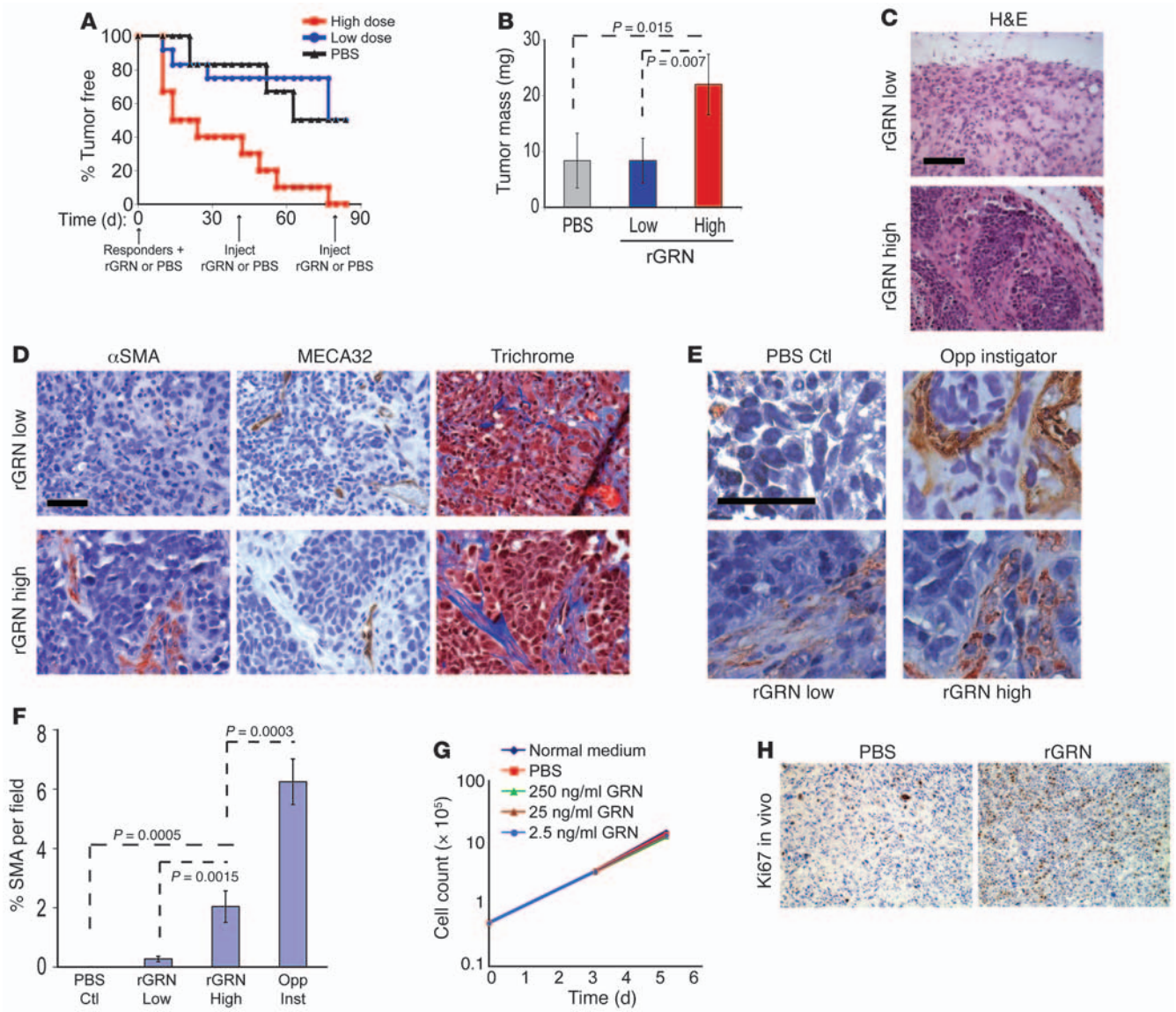


**Figure 5**

GRN treatment mimics systemic instigation and results in responding tumor growth in vivo. (**A**) Responding tumor incidence following injection and in situ treatment with rGRN protein at a high dose (250–2500 ng/ml) or low dose (2.5–25 ng/ml) or PBS control. Subcutaneous tumor sites were treated as indicated with 2 additional injections ($n$ = 12 per group). (**B**) Average final mass of tumors represented in **A**. (**C**) Representative H&E staining of tumors treated with high or low dose of rGRN; cell nuclei stain dark purple. Scale bar: 100 μm. (**D**) Representative immunohistochemical staining of tumors treated with high or lose dose of rGRN. Serial tumor sections were stained for αSMA (red, left), mouse endothelial cell antigen (MECA32, brown, center), and Masson's trichrome staining for collagen (blue, right). Scale bar: 50 μm. (**E**) Representative images used to quantify the extent of αSMA (red) incorporated into responding tumors that grew either opposite instigating tumors, in the presence of high or low dose rGRN, or with PBS control; cell nuclei were counterstained with hematoxylin (blue). Scale bar: 50 μm. Outlines show αSMA⁺ staining as identified by CellProfiler software (see Methods). (**F**) Graph shows average image area occupied by αSMA staining analyzed on a minimum of 25 images representing 5 tumors per group. (**G**) Growth of responding tumor cells in vitro during daily treatment with indicated doses of rGRN or PBS control. (**H**) Images of responding tumors resulting from either PBS control or high dose rGRN treatment and stained for proliferation marker Ki67 (brown); nuclei are counterstained with hematoxylin (blue). Original magnification, ×100. Data are expressed as mean ± SEM.

mice, GFP⁺ myofibroblasts were extremely rare in these tumors (Figure 2E); we also found this to be true of the stroma of instigating tumors. Thus, when we counted GFP⁺αSMA⁺ cells under the confocal microscope, we observed that none of the stromal myofibroblasts were derived from the BM in the 2 different instigating tumor types that we examined (not shown). These observations indicated that the BMCs present in instigated tumor stroma did not serve as direct precursors of stroma-associated myofibroblasts. Instead, these recruited BMCs played another role in stromal development, such as facilitating the recruitment and/or transdifferentiation of myofibroblasts from nearby tissues.

*Identification of instigating BM cells.* For these reasons, we attempted to identify the specific subtype or subtypes of BMCs that were responsible for the effects of systemic instigation. We previously

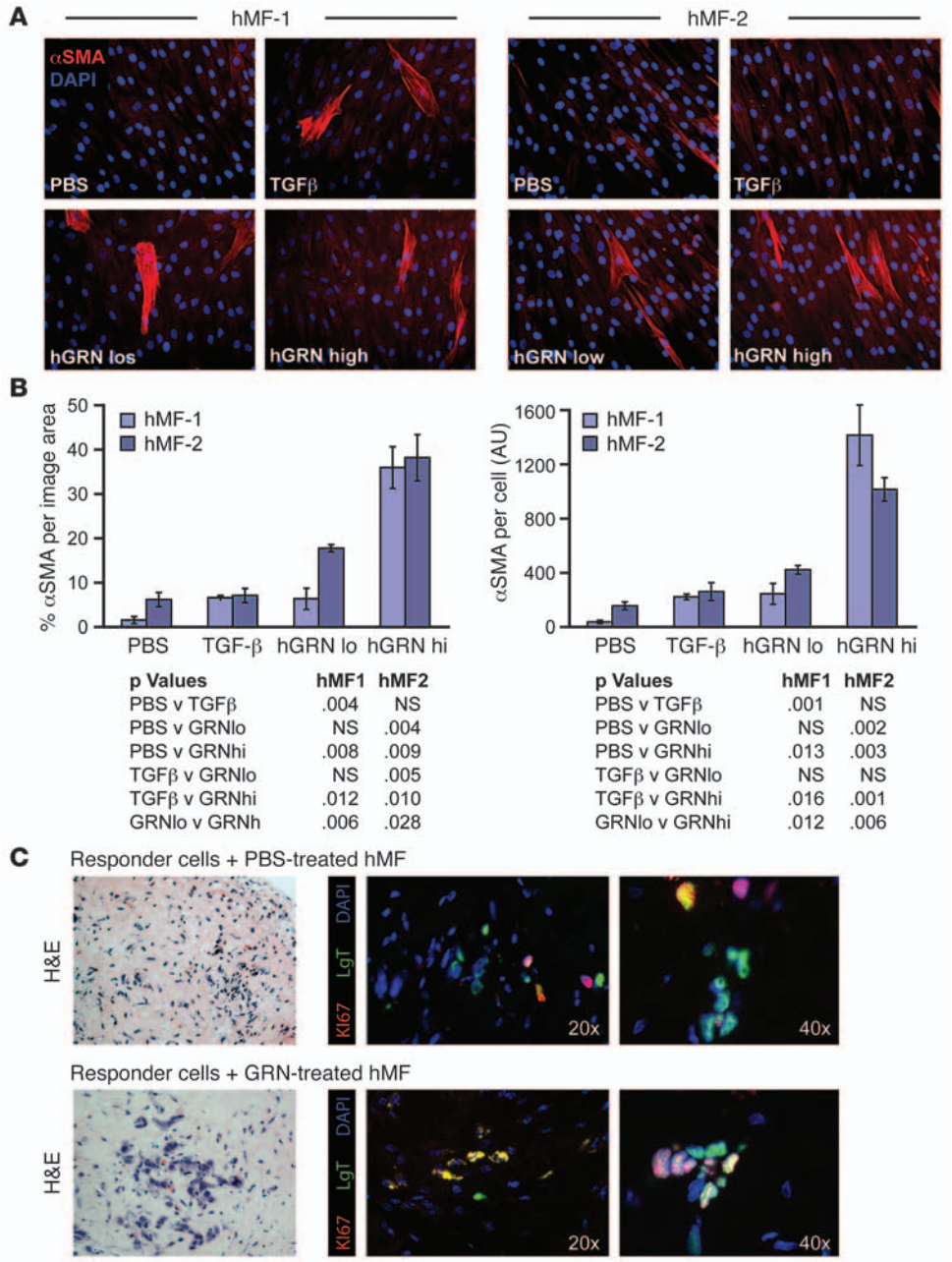


**Figure 6**
GRN induces αSMA expression in human mammary fibroblasts and affects tumor growth. (**A**) Images show 2 different preparations of cultured normal human mammary fibroblasts (hMF-1 and hMF-2; isolated from patients undergoing reduction mammoplasty) following 6-day treatment with 5 ng/ml recombinant human TGF-β-1, human GRN protein (hGRN) at a low dose (250 ng/ml) or high dose (1 μg/ml), or PBS control. Treated cells were stained for αSMA (red); cell nuclei were stained with DAPI (blue). Original magnification, ×200. (**B**) Graphs representing CellProfiler quantification of αSMA staining in cultured human mammary fibroblasts from **A** following indicated treatments. Left: average percentage of total image area occupied by αSMA$^+$ staining. Right: average αSMA staining per cell (arbitrary units) as calculated by total αSMA$^+$ pixel area divided by number of cell nuclei counted in each image by CellProfiler software. $n$ = 6 images per group; $P$ values indicated below graphs. Data are expressed as mean ± SEM. (**C**) Representative images of responding tumors resulting from injection of admixtures of responder cells with human mammary fibroblasts that had been pretreated with PBS (top) or GRN (bottom). Left: H&E stains of responding tumor sections. Original magnification, ×20. Center and right: merged images of tumor sections stained for the SV40 LgT (green) to visualize responder cells, Ki67 (red) to visualize proliferating cells, and DAPI to mark cell nuclei. Yellow indicates proliferating responding tumor cells.

reported that Sca1$^+$cKit$^-$ BMCs were the most abundant BM-derived cell type incorporated into the responding tumors that had been stimulated by instigating tumors. Moreover, Sca1$^+$cKit$^-$ BMCs were incorporated in significantly greater numbers into the stroma of responding tumors implanted contralaterally to instigating tumors than those that were implanted opposite control or noninstigating tumors (9). At the same time, we reported that Lin$^-$Sca1$^+$cKit$^+$ BMCs were reduced in numbers in the marrow of mice bearing instigating tumors as compared with control hosts.

To further characterize these various BMC subpopulations, we harvested cells from the marrow of mice bearing instigating tumors and fractionated them by FACS into Sca1$^+$cKit$^-$, Sca1$^+$cKit$^+$, and Sca1-depleted fractions (Figure 3A). We then mixed each of these distinct BMC subpopulations separately with responding tumor cells and implanted the cell mixtures into mice to determine whether any of these subpopulations could participate in the formation of tumor stroma and accelerate responding tumor growth. Importantly, we mixed these various BMC subtypes in numbers that reflected their relative representation in the whole unfractionated BM.

When we mixed either $7.5 \times 10^3$ Sca1$^+$cKit$^+$ (Figure 3A) or $7.25 \times 10^5$ Sca1-depleted cells (Figure 3A) with $2.5 \times 10^5$ responder cells prior to injection into host mice, we found that neither population was capable of enhancing responding tumor growth to any significant extent above that of responder cells implanted on their own (Figure 3B). In fact, the few tumor masses that we recovered from such cell mixtures exhibited nondesmoplastic stroma with areas of necrosis and edema (Figure 3C).

**Table 1**
Summary of enriched gene sets in granulin-treated fibroblasts

**Cytokine- and chemokine-related pathways (pZC = 3.7e-005)**

| Gene symbol | Gene name | Gene ID | Fold change | q |
|---|---|---|---|---|
| *IL8* | Interleukin 8 | 3576 | 54.34975 | 0.00446 |
| *IL1B* | Interleukin 1, beta | 3553 | 36.81125 | 0.00446 |
| *CCL2* | Chemokine (C-C motif) ligand 2 | 6347 | 35.77197 | 0.00446 |
| *CXCL3* | Chemokine (C-X-C motif) ligand 3 | 2921 | 27.26983 | 0.00533 |
| *CCRL1* | Chemokine (C-C motif) receptor-like 1 | 51554 | 23.57727 | 0.00561 |
| *CXCL1* | Chemokine (C-X-C motif) ligand 1 | 2919 | 21.29913 | 0.00598 |
| *IL1R1* | Interleukin 1 receptor, type I | 3554 | 17.36243 | 0.00773 |
| *IL1A* | Interleukin 1, alpha | 3552 | 16.15399 | 0.00830 |
| *CXCL2* | Chemokine (C-X-C motif) ligand 2 | 2920 | 15.63894 | 0.00878 |
| *TNFRSF19* | Tumor necrosis factor receptor superfamily, 19 | 55504 | 14.90488 | 0.00940 |
| *IFNAR2* | Interferon (alpha, beta, and omega) receptor 2 | 3455 | 11.74451 | 0.01284 |
| *TGFBR3* | Transforming growth factor, beta receptor III | 7049 | 11.73960 | 0.01284 |
| *IL1RN* | Interleukin 1 receptor antagonist | 3557 | 10.51175 | 0.01526 |
| *TGFBR1* | Transforming growth factor, beta receptor 1 | 7046 | 8.12137 | 0.02263 |
| *ACVR1* | Activin A receptor, type I | 90 | 7.80661 | 0.02400 |
| *IRS2* | Insulin receptor substrate 2 | 8660 | 7.74296 | 0.02415 |
| *ACVR2A* | Activin A receptor, type IIA | 92 | 7.00928 | 0.02811 |
| *IL10RB* | Interleukin 10 receptor, beta | 3588 | 6.94320 | 0.02844 |
| *IL6* | Interleukin 6 (interferon, beta 2) | 3569 | 6.19520 | 0.03495 |

**Integrin signaling (pZC = 2.9e-005)**

| Gene symbol | Gene name | Gene ID | Fold change | q |
|---|---|---|---|---|
| *COL4A5* | Collagen, type IV, alpha 5 | 1287 | 25.99393 | 0.00533 |
| *LYN* | Yamaguchi sarcoma viral-related oncogene | 4067 | 18.03796 | 0.00745 |
| *ITGB8* | Integrin, beta 8 | 3696 | 17.73816 | 0.00761 |
| *ITGA2* | Integrin, alpha 2 (CD49B, alpha 2 subunit VLA2R) | 3673 | 16.32564 | 0.00816 |
| *LAMB1* | Laminin, beta 1 | 3912 | 16.24468 | 0.00824 |
| *PIK3R1* | Phosphoinositide-3-kinase, regulatory subunit 1 | 5295 | 15.57327 | 0.00878 |
| *NTN4* | Netrin 4 | 59277 | 12.93177 | 0.01133 |
| *COL3A1* | Collagen, type III, alpha 1 | 1281 | 12.47467 | 0.01195 |
| *COL6A2* | Collagen, type VI, alpha 2 | 1292 | 12.39645 | 0.01195 |
| *COL12A1* | Collagen, type XII, alpha 1 | 1303 | 12.11785 | 0.01231 |
| *ITGBL1* | Integrin, beta-like 1 (EGF-like repeat domains) | 9358 | 11.76166 | 0.01284 |
| *LAMC1* | Laminin, gamma 1 (formerly LAMB2) | 3915 | 11.09913 | 0.01429 |
| *FYN* | FYN Oncogene related to SRC, FGR, YES | 2534 | 10.06980 | 0.01648 |
| *COL16A1* | Collagen, type XVI, alpha 1 | 1307 | 9.90975 | 0.01691 |
| *COL5A3* | Collagen, type V, alpha 3 | 50509 | 9.61834 | 0.01759 |
| *LAMA4* | Laminin, alpha 4 | 3910 | 9.27839 | 0.01851 |
| *COL5A1* | Collagen, type V, alpha 1 | 1289 | 8.78712 | 0.02032 |
| *CAV1* | Caveolin 1, caveolae protein, 22 kDa | 857 | 8.50090 | 0.02153 |
| *COL6A3* | Collagen, type VI, alpha 3 | 1293 | 8.20476 | 0.02246 |
| *PARVA* | Parvin, alpha | 55742 | 8.13141 | 0.02263 |
| *COL7A1* | Collagen, type VII, alpha 1 | 1294 | 8.11981 | 0.02263 |
| *PIK3C2A* | Phosphoinositide-3-kinase, class 2, alpha | 5286 | 7.98190 | 0.02312 |
| *ITGAE* | Integrin, alpha E (CD103) | 3682 | 7.75790 | 0.02415 |
| *DOCK5* | Dedicator of cytokinesis 5 | 80005 | 6.98370 | 0.02816 |
| *SOS1* | Son of sevenless homolog 1 (Drosophila) | 6654 | 6.42290 | 0.03280 |
| *COL6A1* | Collagen, type VI, alpha 1 | 1291 | 6.31893 | 0.03375 |

GRN induces inflammation and matrix remodeling gene expression signatures in human mammary fibroblasts. Summary of gene sets enriched in human mammary fibroblasts treated with human rGRN (1 μg/ml) every 24 hours for 6 days as compared with control PBS treatment. Samples analyzed in triplicate. pZC denotes the *P* value computed using the Zhang C statistic; q denotes *P* value corrected for multiple testing.

In striking contrast, as few as $2.5 \times 10^4$ admixed Sca1$^+$cKit$^-$ BMCs from instigator-bearing mice (Figure 3A) enhanced the growth of responding tumors, yielding tumors that were approximately 6-fold larger than masses formed from responding tumor cells implanted on their own (Figure 3B). The responding tumors that grew as a result of admixture of these Sca1$^+$cKit$^-$ BMCs acquired a desmoplastic stroma in which αSMA$^+$ myofibroblasts and collagen were uniformly and widely distributed (Figure 3C).

We therefore concluded that the tumor-promoting activity of the BM from instigator-bearing mice was attributable to the presence of an instigating Sca1$^+$cKit$^-$ subpopulation of BMCs. Lin$^-$Sca1$^+$cKit$^-$ cells have been described previously as a population of hematopoietic progenitor cells of unknown function (25, 26). Some reports suggest that various subsets of Sca1$^+$cKit$^-$ cells can give rise to both lymphoid- and myeloid-biased precursors (27–29). We wished to determine whether the tumor-promoting activity of these Sca1$^+$cKit$^-$ BMCs was unique to instigator-bearing mice, or whether, alternatively, the comparable population from control mice might exhibit this activity. First, we discovered that the representation of the Sca1$^+$cKit$^-$ subpopulation was similar in the BM of tumor-bearing and control mice and that these cells represented less than approximately 2% of the total BM cellularity in all cases (Figure 3D). Accordingly, we sorted the Sca1$^+$cKit$^-$ population from control Matrigel or noninstigator bearing mice (Figure 3A) and mixed $2.5 \times 10^4$ of these cells with responder cells prior to implantation in host mice. Unlike the Sca1$^+$cKit$^-$ BMCs from instigator-bearing mice, which had potent tumor-promoting ability, the same number of Sca1$^+$cKit$^-$ BMCs from the marrow of mice bearing size-matched noninstigating tumors lacked this ability (Figure 3B). Thus, the control Sca1$^+$cKit$^-$ BMCs did not enhance responding tumor incidence or size above that of the responder cells implanted on their own. Moreover, the few, small resulting responding masses that did form displayed a nondesmoplastic stroma (Figure 3C).

These observations indicated that the overall size of the Sca1$^+$cKit$^-$ BMC compartment was not affected by the presence

**Table 2**
Correlations between GRN expression and clinicopathologic features of patient breast tumors

| | Correlation coefficient | *P* value (2-tailed) | N |
|---|---|---|---|
| Age | 0.111[A] | 0.215 | 126 |
| Tumor size | 0.362[B] | 0.000 | 126 |
| Grade | 0.347[B] | 0.000 | 126 |
| Nodal stage | 0.13[A] | 0.168 | 114 |
| Histological subtype | –0.246[C] | 0.005 | 126 |
| Her 2 status | 0.128[A] | 0.157 | 123 |
| Her 2 subtype | 0.045[A] | 0.619 | 123 |
| Manual ER status | –0.255[C] | 0.004 | 126 |
| Manual PR status | –0.212[C] | 0.017 | 126 |
| Triple negative | 0.291[B] | 0.001 | 123 |
| Molecular subtype | 0.224[B] | 0.012 | 126 |
| Luminal B | 0.014[A] | 0.879 | 123 |
| Luminal A | –0.268[C] | 0.003 | 120 |
| Basal | 0.291[B] | 0.001 | 123 |
| Ki67 3g | 0.321[B] | 0.001 | 109 |

Data shown are for analysis of GRN staining on TMAs using antibody HPA028747. [A]No significant correlation. [B]Statistically significant positive correlations. [C]Negative correlation.

of an instigating tumor, but that a subpopulation of cells in this compartment was functionally changed under conditions of systemic instigation. Therefore, we undertook to determine whether use of other cell-surface markers would allow us to identify the instigating BMC subtype with even greater precision. When comparing BMCs from instigator-bearing hosts to those of control Matrigel– or noninstigator-bearing hosts, flow cytometric analyses revealed no significant differences in the representation of $Sca1^+cKit^-$ BMCs that bore additional, commonly studied cell-surface markers (Figure 3E). In the marrow from all groups of mice, approximately 95% of the $Sca1^+cKit^-$ BMCs were CD45 positive, indicating that the majority of these cells were of hematopoietic origin (Figure 3E). In addition, there were no significant differences in the composition of the $Sca1^+cKit^-$ BMCs among groups of mice when we examined cell-surface expression of the CD11b (~4%), CD11c (~9%), VEGFR1 (~2%), Gr1 (~3%), $CD11b^+CD45^+$ (~4%), $CD11b^+Gr1^+$ (~2%), and NK1.1 (~1%) markers (Figure 3E).

Taken together, these results revealed that (a) the $Sca1^+cKit^-CD45^+$ subpopulation of BMCs from hosts bearing instigating tumors is highly enriched for the functional activity that promotes responding tumor growth; (b) BMCs exhibiting the $Sca1^+cKit^-CD45^+$ profile, although equally represented in number in the BM of all groups of mice, differed in their biological activity when prepared from the BM of instigator-bearing hosts relative to the BM of control hosts; and (c) analysis of commonly studied cell-surface antigens did not allow us to further resolve the subpopulation of BMCs within the $Sca1^+cKit^-$ population that was responsible for systemic instigation.

*Unique expression profile of instigating $Sca1^+cKit^-$ BMCs.* Since $Sca1^+cKit^-$ BMCs from instigator-bearing and control mice were similar in their cell-surface antigen profiles, we sought other means to uncover possible changes in this subpopulation of cells that occur in response to systemic instigation. More specifically, we speculated that differences in gene expression might provide clues about their differing instigating abilities. Accordingly, we obtained gene expression profiles of FACS-sorted $Sca1^+cKit^-$ BMCs from mice bearing instigating tumors and size-matched noninstigating tumors in order to identify genes that might be associated specifically with the instigating activity.

Analysis of the expression array data identified genes that were expressed at significantly different levels in the instigating $Sca1^+cKit^-$ BMCs compared with their noninstigating counterparts (GEO GSE25620). The most differentially expressed gene ($t$ = 5.3) was granulin (GRN, also termed granulin-epithelin precursor, proepithelin, acrogranin, or PC cell–derived growth factor) (Figure 3F). GRN belongs to the epithelin family of secreted growth factors and is expressed by numerous cell types, including hematopoietic cells, epithelial cells, and certain neurons (30). GRN has been shown to mediate inflammation, developmental cavitation, and wound healing and is highly expressed in surgical samples from patients with aggressive cancers (30). We validated these results in a larger number of samples by quantitative PCR and determined that *GRN* mRNA was significantly upregulated, approximately 2.5-fold, in instigating $Sca1^+cKit^-$ BMCs relative to the counterpart BMCs prepared from Matrigel-bearing control mice, which lack instigating ability (Figure 2G).

Our analyses indicate that instigating tumors, even in the absence of metastasis to the BM, activate specific gene expression programs in a subset of hematopoietic BMCs, while noninstigating tumors fail to do so. Because GRN was the most differentially expressed of these genes, we wished to determine whether GRN-expressing BMCs are recruited into the responding tumors and, if so, what role GRN might play in responding tumor instigation.

*GRN-expressing BMCs in responding tumor stroma and GRN in host plasma.* We first asked whether host-derived GRN was evident in the tumors resulting from the admixture of responder cells with the instigating $Sca1^+cKit^-$ BMCs — the class of cells in which we had identified upregulated GRN expression in the BM. Indeed, when $Sca1^+cKit^-$ cells from the BM of instigator-bearing mice were mixed with the responder cells, the resulting tumors were highly positive for GRN (Figure 4A). The $GRN^+$ cells in these tumors were also positive for Sca1 (Figure 4C), indicating that the admixed BMCs provided the source of host-derived GRN that we observed in these tumors.

In contrast, when $Sca1^+cKit^-$ cells from the BM of Matrigel-implanted control mice were admixed, the resulting tumors displayed little, if any, GRN staining (Figure 4A). In fact, the extent of GRN positivity was approximately 5-fold higher in the tumors resulting from admixture of instigating BMCs as compared with the control BMCs ($P < 0.01$; Figure 4A). In this experiment, we could not include analysis of tumors resulting from admixture of BMCs from noninstigator-bearing mice, as such BMCs did not yield any responding tumors. Nonetheless, it was apparent that GRN positivity in responding tumors correlated well with the instigating ability of the BMCs that had been mixed with responding cells prior to implantation.

We wondered whether GRN-positive host BMCs were also recruited into the responding tumors that grew as a result of systemic instigation by contralaterally implanted instigating tumors. Responder cell masses that were implanted contralaterally to control Matrigel plugs displayed very little GRN positivity (Figure 4B). In marked contrast, the total stromal area marked by positive GRN staining was approximately 5-fold greater in the responding tumors that had grown opposite BPLER instigating tumors than was present in those implanted opposite Matrigel control plugs ($P < 0.01$; Figure 4B). Separate experiments conducted in mouse hosts that

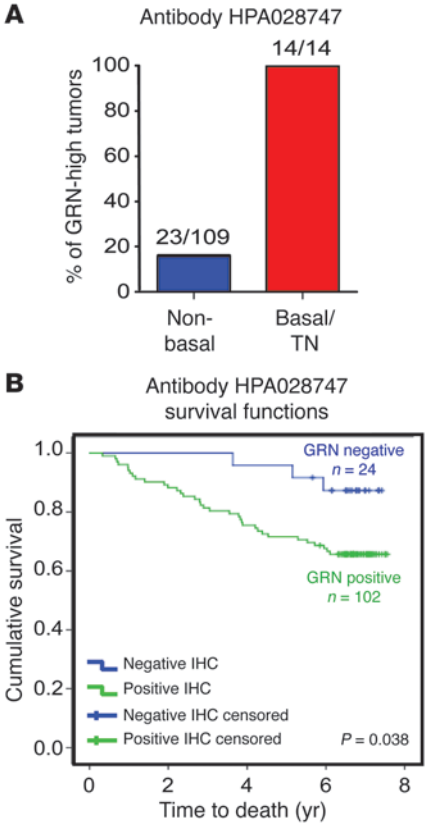


**Figure 7**
GRN expression correlates with aggressive tumor subtypes and reduced survival of breast cancer patients. (**A**) Percentage of tumors in each category (triple-negative [TN]/basal or nonbasal) that scored positively for high GRN staining using antibody HPA028747. (**B**) Kaplan-Meier analysis of correlation between GRN-positive (green) or GRN-negative (blue) expression and survival.

had been transplanted previously with GFP$^+$ BMCs confirmed that GFP/GRN double-positive cells were indeed incorporated into the stroma of responding tumors that had grown opposite the instigating tumors (Supplemental Figure 4A), indicating that recruited BMCs provided a source of host GRN in these tumors.

We also examined the responding tumors early in the instigation process, 4 weeks after responding tumor implantation. We found that the Sca1-positive cells recruited into these instigated tumors also expressed GRN (Figure 4C). This prompted us to examine the small tissue plugs that we recovered opposite noninstigating tumors 4 weeks after implantation. We found that there were no GRN-positive cells in these noninstigated plugs, as compared with a significant number of GRN-positive cells observed in the responding tumor tissues after 4 weeks of exposure to the instigating systemic environment (Supplemental Figure 4B).

We then undertook to determine how GRN staining in the stroma of these instigated tumors related to the localization of αSMA-positive cells since, as described above, in the presence of contralateral instigating tumors, responding tumors formed desmoplastic stroma rich in αSMA-positive myofibroblasts. In fact, we observed that GRN-positive cells were largely confined to the stromal compartments of responding tumors and were localized near the αSMA$^+$ myofibroblasts; importantly, however, GRN staining did not colocalize with αSMA staining (Figure 4, D–F). We also observed similar staining patterns in the contralateral instigating tumors (Supplemental Figure 4C).

The fact that instigating tumors stimulated host Sca1$^+$cKit$^-$ BMCs to secrete GRN led us to examine whether we could detect murine GRN in the host plasma. We detected approximately 1.5- to 2-fold elevations of GRN in the plasma of mice bearing instigating tumors above that of mice bearing control Matrigel or noninstigating tumors ($P < 0.05$; Figure 4G). Although the precise source of the plasma GRN could not be determined, these results suggest that elevated plasma GRN levels indicate the presence of activated BMCs in the circulation of instigating tumor-bearing hosts.

Collectively, these results indicated that GRN-positive Sca1$^+$ BM–derived cells are recruited, via the circulation, into responding tumors only under instigating conditions. These GRN-expressing BMCs do not give rise to stromal myofibroblasts and confirmed our earlier observation that the great majority of the myofibroblasts in the stroma of instigating and responding tumors do not originate in the BM.

*Effect of GRN on responding tumor growth.* Our results, as described above, indicated that instigating tumors stimulate GRN expression within the Sca1$^+$cKit$^-$ fraction of hematopoietic BMCs prior to their mobilization into the general circulation and that many GRN-positive cells are subsequently found in the stroma of indolent tumors. We speculated that GRN secretion by these BM-derived cells might play a causal role in some aspect of systemic instigation, specifically in the development of the stromal desmoplasia in the instigated tumors. Accordingly, we tested whether soluble, recombinant pro-GRN (rGRN) protein would affect responding tumor growth and mimic systemic instigation. To do so, we subcutaneously implanted indolent tumor cells in Matrigel impregnated with various doses of rGRN (250 ng/ml and 2500 ng/ml, collectively referred to as high-dose rGRN; 2.5 ng/ml and 25 ng/ml, collectively referred to as low-dose rGRN). Moreover, throughout the experimental time course, we periodically administered injections of rGRN directly into the subcutaneous sites where responding tumor cells had previously been implanted.

Within 14 days, 50% of the responding cell implants treated with high-dose rGRN had formed externally palpable tumors, while only 17% of the low-dose rGRN and none of the PBS-treated cells did so (Figure 5A). By 77 days, 100% of the high-dose rGRN-treated responder cells had formed tumors, while only 50% of the low-dose rGRN and PBS-treated sites formed palpable masses (Figure 5A). At the experimental end point, the average final mass of the high-dose rGRN-treated tumors was significantly higher (2.7-fold) than that of the low-dose rGRN and PBS-treated tumors ($P < 0.05$; Figure 5B). We note here that comparable increases in the overall tumor mass have been observed by us repeatedly in the context of systemic instigation (9).

rGRN treatment also had a profound effect on the histopathology of the responding tumors. The cell plugs recovered from sites injected with either low doses of rGRN contained viable responder cells; however, these tumor cells appeared to form benign masses that did not resemble carcinomas (Figure 5C). These responding tumors did not contain αSMA$^+$ cells and displayed little if any collagen deposition in their stroma (Figure 5D). Staining these tissues with anti-MECA32 antibody revealed that blood vessels were present within these masses (Figure 5D).

In striking contrast, the responder cells recovered from sites injected with high doses of rGRN formed tumors with a histopathology consistent with adenocarcinomas (Figure 5C). These

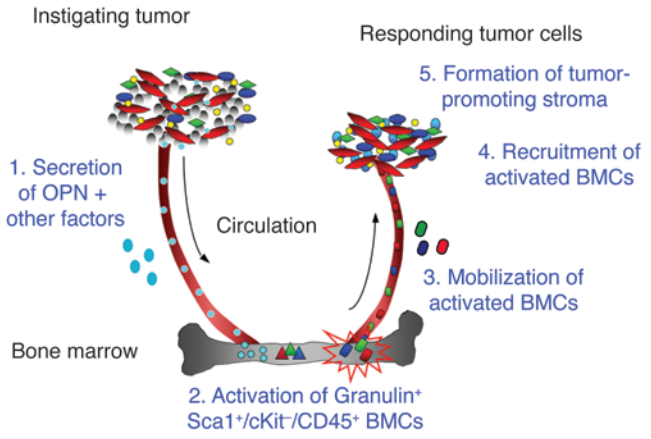


**Figure 8**

The systemic instigation model. Instigating tumors secrete endocrine factors, including but not limited to OPN (9), that mediate the expression of GRN by Sca1$^+$cKit$^-$CD45$^+$ hematopoietic cells in the host BM. These activated BMCs are subsequently mobilized into the circulation and are recruited to sites where otherwise indolent responding tumors reside. The GRN-expressing BMCs assume close proximity to tissue fibroblasts within the tumor stroma and induce these fibroblasts to express αSMA as well as genes related to cytokine- and chemokine-mediated inflammation, integrin signaling, and matrix remodeling. This systemic instigation cascade ultimately results in malignant growth of the responding tumors.

tumors contained both αSMA$^+$ cells and collagen that were deposited throughout the tumor-associated stroma (Figure 5D). Moreover, very few of the αSMA$^+$ cells in these tumors localized with MECA32$^+$ cells, suggesting that the majority of these cells were myofibroblasts and not pericytes (Figure 5D).

In further support for a role of GRN in mediating desmoplasia, the extent of αSMA positivity in resulting tumors correlated well with the dose of rGRN that had been administered. CellProfiler image analysis (18, 19) revealed that 0.26% of the responding tumor surface area was covered by positive staining for αSMA in the responding tumors treated with low-dose rGRN (Figure 5, E and F), while in the PBS-treated tumors, αSMA accounted for only 0.01% of the imaged tumor surface area ($P = 0.005$). Administration of high-dose rGRN resulted in 2% coverage of tumor surface area by αSMA positivity; this level was significantly above that of both PBS ($P = 0.0005$) and low-dose rGRN treatment ($P = 0.0015$; Figure 5, E and F). Nonetheless, the responding tumors treated with high dose rGRN did not achieve the same extent of αSMA coverage as those responders that grew opposite instigating tumors (6.2%; $P < 0.001$; Figure 5, E and F).

In vitro studies showed that introduction of recombinant GRN, at any dose, into culture media did not affect the proliferation of responder cell populations (Figure 5G); in contrast, the responder cells in the tumors that formed in vivo upon GRN treatment were highly proliferative, as determined by staining for the Ki67 proliferation marker (Figure 5H). Collectively, these results demonstrate that GRN protein increases the frequency of responding tumor formation, significantly enhances responding tumor mass, and facilitates the formation of stromal desmoplasia. In addition, they suggest that the effects of GRN on responder cells are not direct and could only be manifested in vivo. Hence, GRN secretion in the responding tumors could, on its own, phenocopy most of the effects elicited by contralateral instigating tumors.

*Effect of GRN on human mammary fibroblasts.* Our data support the notion that secretion of GRN by tumor-associated Sca1$^+$cKit$^-$ hematopoietic BM-derived cells phenocopies the key aspects of systemic instigation (i.e., outgrowth of indolent tumors and development of stromal desmoplasia). This suggested that the formation of the myofibroblasts might well arise through the GRN-induced transdifferentiation of existing fibroblasts residing in the tumor stroma or in adjacent normal tissue. Accordingly, we set up a series of cell culture experiments to examine the effects of human rGRN on human mammary stromal fibroblasts.

We cultured 2 different preparations of normal human mammary fibroblasts (hMF-1 and hMF-2) in the presence of various doses of human rGRN. Both populations of these fibroblasts had been isolated from patients undergoing reduction mammoplasty. We found that GRN enhanced expression of αSMA by human mammary fibroblasts in a dose-dependent manner (Figure 6, A and B). Both hMF-1 and hMF-2 treated with high-dose rGRN (1 μg/ml) exhibited significant increases in αSMA expression that were 23.9-fold ($P = 0.008$) and 6.2-fold ($P = 0.009$) higher, respectively, than that of PBS control–treated cultures (Figure 6B and Supplemental Figure 5A). In fact, in both cases, these levels of αSMA expression were significantly higher than that observed with 5 ng/ml recombinant TGF-β treatment ($P = 0.01$ each), which has been reported to induce αSMA expression in cancer-associated fibroblasts (CAFs) (31, 32) but had only a minor effect in our experiments. Consistent with our observations of the αSMA$^+$ myofibroblast–rich responding tumors, we also confirmed that murine GRN significantly upregulated expression of αSMA in a dose-dependent fashion in mouse fibroblasts in vitro (Supplemental Figure 5B). Both normal fibroblasts and CAFs are heterogeneous, and different types of CAFs are thought to make distinct functional contributions to tumor growth (33–37). Moreover, markers that are shared in common by all fibroblasts have not been defined. Therefore, to investigate how GRN impinges upon fibroblast function beyond induction of αSMA expression, we treated triplicate samples of hMF-2 human mammary fibroblasts with either human rGRN (1 μg/ml) or PBS control every 24 hours for 6 days, prepared mRNA, and performed gene expression microarray analysis (Affymetrix U133 Plus).

We computed differentially expressed genes between rGRN-treated fibroblasts and PBS-treated fibroblasts and identified 138 differentially expressed probe sets (false discovery rate < 1%). Among the top genes induced in response to rGRN treatment, we observed several inflammatory cytokines and chemokines, including *CXCL2*, *IL6*, *IL1B*, *CXCL1*, *IL8*, *CCL2*, *IL1A*, *CXCL3*, *CCRL1*, *CXCL6* (Table 1; GEO GSE25619). Many of these genes have been recently included in a proinflammatory gene expression signature that was generated from the analysis of CAFs in mouse models of skin, mammary, and pancreatic cancers as well as in the cognate human cancers (37).

Enrichment testing against gene set collections provided by the Gene Ontology Consortium and Applied Biosystems revealed that gene sets related to cytokine- and chemokine-related immunity were enriched in the genes that were upregulated by GRN treatment (pZC < 0.0001; Table 1). In addition to these proinflammatory genes, the GRN-induced expression signature was enriched for genes that mediate integrin signaling (including laminins and various collagens) in our primary human mammary fibroblasts (pZC < 0.0004; Table 1).

*Effect of GRN-treated fibroblasts on tumor growth.* To explore whether GRN-actived fibroblasts can initiate responding tumor growth in vivo, we pretreated normal human mammary fibroblasts with

GRN in vitro for a period of 6 days and then mixed them with responder cells in a ratio of 1:1 prior to injection into host mice. As a control, we made preparations of these fibroblasts that had been exposed to PBS and injected an admixture of these control fibroblasts and responding tumor cells. We then evaluated responding tumor formation and histopathology 2 weeks after injection of these tumor/fibroblast admixtures.

We observed that fibroblasts activated ex vivo by GRN exposure subsequently enabled formation of responding tumor foci that histopathologically resembled neoplastic breast tumors (Figure 6C). Within these masses, the responding tumor cells were indeed proliferative, as indicated by costaining for the LgT (expressed exclusively by the tumor cells) and the proliferation marker Ki67 (Figure 6C). In contrast, normal mammary fibroblasts exposed ex vivo to PBS and then admixed to responder cells prior to implantation yielded disorganized masses, with significantly fewer proliferating tumor cells (Figure 6C). In vitro studies of tumor responder cells cocultured with GRN-activated fibroblasts did not mimic these in vivo phenomena and did not induce responder cell proliferation (Supplemental Figure 6).

Collectively, these analyses indicate that instigating GRN-expressing $Sca1^+cKit^-$ hematopoietic cells recruited to sites in which responding tumor cells reside function to induce a local inflammatory response and remodel the extracellular milieu through paracrine interactions with resident fibroblasts. The resulting transdifferentiation of the latter into myofibroblasts appears to contribute in a major way to enabling the growth of tumors that would otherwise remain indolent.

*GRN expression is correlated with aggressive tumor subtypes and poor survival of breast cancer patients*. In the context of cancer pathogenesis, GRN has been described as an autocrine growth factor that is expressed by tumor epithelial cells and enhances tumorigenicity in vitro and in vivo (38–42). Nevertheless, the consequences of GRN expression and its relevance to breast cancer tumor types and patient survival have been unclear.

Accordingly, we analyzed GRN expression in tissue microarrays (TMA) assembled from tumors arising in a cohort of 144 patients diagnosed with breast cancers of various grades, stages, receptor status, and subtypes (Supplemental Table 1). To do so, we used 3 different antibodies to GRN protein: CAB019394, HPA028747, and HPA008763. HPA antibodies were specifically generated and used for protein profiling as part of the Human Protein Atlas effort (http://www.proteinatlas.org) (43). All tissues were analyzed in a blinded fashion with nonbiased acquisition of expression results. For each antibody, we performed CellProfiler image analysis to calculate the total area of each tissue section that was occupied by high GRN staining (highest intensity of positive GRN staining; Supplemental Figure 7).

The absolute values of GRN staining area among the 3 different antibodies, while not identical, were in good agreement (Supplemental Figure 8A). Statistical analyses revealed that the extent of high GRN staining was positively correlated with tumor size ($P < 0.038$) for all 3 antibodies and with grade for 2 of the 3 antibodies ($P < 0.001$), but not with nodal stage for any of the antibodies tested (Table 2 and Supplemental Figure 8B). GRN expression was also significantly correlated with histological and molecular subtypes of breast cancer. Specifically, high GRN expression negatively correlated with the luminal A subtype and positively correlated with triple negative and basal-like breast cancer subtypes for all 3 of the antibodies we tested (Table 2 and Supplemental Figure 8B).

Further analysis of the tissues stained with the HPA028747 antibody indicated that high GRN expression was positively correlated with the proliferation index, as indicated by Ki67 positivity ($P = 0.001$), while being negatively correlated with ER ($P = 0.004$) and PR status ($P = 0.017$; Table 2). GRN expression was strongly correlated with the triple-negative/basal-like breast tumor subtypes ($P = 0.001$; Table 2). In fact, 100% of the triple-negative/basal-like tumors expressed high GRN levels, while only 16% of the luminal tumors displayed similar levels of GRN expression (Figure 7A). In this case, breast cancer patients with tumors that were positive for GRN staining showed significantly worse outcome in overall survival (HPA028747, $P = 0.038$; Figure 7B). Together, these observations are in accord with reports that patients with triple-negative tumors have worse outcome, distinctive patterns of relapse, and reduced survival (44–46).

## Discussion

The importance of the tumor microenvironment has been appreciated for at least 5 decades (47), and it is now widely accepted that many of the tumor microenvironmental components, notably the stromal fibroblasts and myofibroblasts, actively support tumor growth and progression (reviewed in ref. 48). The formation of stromal desmoplasia involving the presence of $\alpha SMA^+$ myofibroblasts and collagen deposition is a critical event in carcinoma progression and an important prognostic indicator of metastatic disease in cancer patients (13, 49–51). The origins of these CAFs and myofibroblasts have been unclear. Some studies of preclinical animal models and of human cancer patients have implicated the resident fibroblasts in the tissues in which tumors arise (52). Yet others have indicated transdifferentiation of other tissue cell types (17, 23, 53) or the recruitment and subsequent differentiation of circulating or BM-derived cells (22, 54–57). In the present case, repeated observations indicate a local origin of these functionally critical cells, most likely involving the transdifferentiation of resident fibroblasts into myofibroblasts.

Perhaps the most surprising aspect of the instigation process has come from our discovery that the composition of the tumor stroma, in particular the accumulation of tumor-supportive myofibroblasts and the resulting stromal desmoplasia, can be induced in a systemic fashion. These observations indicate that the cellular composition of a tumor is not dictated exclusively by the neoplastic cells themselves. Instead, systemic endocrine signals such as OPN (9) can act upon the BM to exert strong influences on the histopathology and composition of stroma in tumors at distant anatomical sites (Figure 8).

Our findings are in agreement with and extend a recent report of a "proinflammatory signature" expressed by CAFs in experimental models of pancreatic and mammary adenocarcinoma and correlate with genes expressed in human squamous, breast, and pancreatic cancers; however, the study did not reveal the identity of the cells responsible for promoting the proinflammatory fibroblast signature (37). Here, we demonstrate that $Sca1^+cKit^-CD45^+$ hematopoietic cells that are activated in the BM and recruited to responding tumors are responsible for inducing proinflammatory and matrix-remodeling genes in tissue fibroblasts through their secretion of GRN. The precise signaling pathways by which GRN activates proinflammatory and matrix remodeling genes in responding tumor fibroblasts are still unknown, as the cognate cell-surface receptor for GRN has not yet been identified (30). The present observations of in vitro cocultures imply that CAFs express the GRN receptor, which may enable its identification.

Very little is known about native Sca1$^+$cKit$^-$ cells that reside in the BM; primitive Lin$^-$Sca1$^+$cKit$^-$ cells have been described previously as a "mystery population" of hematopoietic cells with debatable marrow-reconstituting capacity and a marked resistance to the cytotoxic effects of 5-FU (25, 26). Other reports suggest that some subsets of Sca1$^+$cKit$^-$ cells represent lymphoid-biased progenitors that do not yet display terminal deoxyribonucleotide transferase or Rag1/2 recombinase activity, while other subsets can give rise to myeloid lineages under certain conditions (27, 28). More recently, Lin$^-$Sca1$^+$cKit$^-$ BMCs have been reported to give rise to all hematopoietic lineages in response to Wnt3a stimulation (29).

Although our analysis of other commonly studied cell-surface antigens expressed by the Sca1$^+$cKit$^-$ BMCs did not reveal differences between instigator- and noninstigator-bearing mice, we noted that expression of the FcγRI — normally expressed on some macrophages, neutrophils, eosinophils, and dendritic cells — was significantly upregulated in our instigating Sca1$^+$cKit$^-$ population (GEO GSE25620). It was recently reported that FcRγ-positive cells are necessary, in a B cell–dependent manner, for malignant progression in a mouse model of squamous carcinogenesis (58). In fact, nude mice like those used in our studies (NCr-*Foxn1$^{nu}$*) do have small numbers of T cell precursors in their BM, mature B cells, mature NK cells, and cells of the myeloid lineages (59, 60). Nevertheless, the relationship between these reported FcRγ cells and the GRN-expressing Sca1$^+$cKit$^-$ hematopoietic cells that we have observed remains to be determined.

We also found large numbers of GRN-expressing BM-derived hematopoietic cells in the responding tumor stroma at early and late stages of responding tumor development, indicating that these BMCs are either continuously recruited or that they persist within the responding tumor mass following their recruitment. Moreover, at present, we do not know the fate of the instigator-activated Sca1$^+$cKit$^-$CD45$^+$ hematopoietic BMCs once they take up residence in the responding tumor stroma. However, importantly, the activated GRN-expressing BMCs recruited into responding tumors do not directly give rise to the tumor-associated myofibroblasts; instead, they mediate stromal activation and facilitate the acquisition of malignant traits in the responding tumor microenvironment.

GRN is correlated with increased malignancy in a number of different cancer types and has been reported to augment tumor cell proliferation in vitro and in vivo (reviewed in ref. 30). A number of reports have demonstrated that GRN is expressed in tumor epithelium as well as tumor stromal compartments (41, 61–64). Indeed, our own survey of tumors from human breast cancer patients revealed areas of GRN staining in both the epithelium and the tumor stroma. While these studies do not reveal the precise source of GRN, it is clear that high GRN expression is significantly associated with the most aggressive breast tumor subtypes and reduced patient survival.

Our work sheds light on a cascade of events with clinically relevant consequences that has been poorly understood — the formation of desmoplastic stroma and malignant growth of otherwise indolent tumors. Noting that the activity of GRN-expressing BMCs is unique to the marrow of hosts bearing instigating tumors, we speculate that effective anticancer therapies might involve targeting GRN or the activated BM-derived hematopoietic cells that express GRN, thereby disrupting these lines of communication that promote cancer progression.

## Methods

*Cell lines*. Generation of HMLER hygro-H-*ras*V12 (responders) and BPLER human mammary epithelial tumor cells (instigators) has been described (9). Human mammary carcinoma MDA-MB-231 (instigators), MDA-MB-436 (noninstigators), and human prostate carcinoma PC3 (noninstigators) were obtained from ATCC and cultured under standard conditions. SUM149 (noninstigators) were provided by Stephen Ethier (University of Michigan, Ann Arbor, Michigan, USA) and grown as described (65).

*Animals and human tumor xenografts*. Female nude mice were purchased from Taconic; Rag1$^{-/-}$eGFPTg mice were previously described (9). All experiments were performed in accordance with regulations of Children's Hospital animal care protocol (09-12-1566) and MIT Committee on Animal Care protocol (1005-076-08). All animal studies were approved by the Children's Hospital Boston (CHB) Animal Care and Use Committee (Boston, Massachusetts). Tumor cells were suspended in 20% Matrigel (BD Biosciences) and injected subcutaneously into nonirradiated mice; tumor diameter was periodically measured on the flanks of live nude mice using calipers; volume was calculated as $4/3\pi r^3$. For systemic instigation experiments, cells were injected contralaterally beneath the skin of nonirradiated recipient mice as follows: $2.5 \times 10^5$ HMLER hygro-H-*ras*V12 was transplanted into the left flank, while $10^6$ GFP$^+$ BPLER, $2.5 \times 10^5$ GFP$^-$ BPLER, $10^6$ MDA-MB-231 (instigators), or $2 \times 10^6$ PC3 (noninstigator) was inoculated in to the right flank.

For experiments to test function of BMCs, BM was harvested from indicated tumor-bearing mice (described below), and either whole BM or FACS-sorted populations were mixed with $2.5 \times 10^5$ HMLER hygro-H-rasV12–responding tumor cells, suspended in 20% Matrigel, and injected subcutaneously into nude mice as previously described (13). The following numbers of BMCs were used: $7.5 \times 10^5$ whole BMCs, $7.5 \times 10^3$ Sca1$^+$cKit$^+$ cells, $7.25 \times 10^5$ Sca1-depleted cells, or $2.5 \times 10^4$ Sca1$^+$cKit$^-$ cells.

*Immunofluorescence and immunohistochemistry*. Dissected tissues were fixed in 4% (w/v) paraformaldehyde 16–18 hours, embedded in paraffin, and sectioned onto ProbeOn Plus microscope slides (Fisher Scientific) for immunohistochemistry or immunofluorescence as described (13). Primary antibodies were as follows: anti-αSMA (1:75, Vector Labs), anti-Ki67 (1:50; BD Biosciences), anti-Sca1 (1:50; BioLegends), anti-GFP (1:400, Abcam), and anti-GRN (1:50, R&D Systems). Secondary antibodies were as follows: FITC–anti-goat IgG (1:100; Abcam), Alexa Fluor 488 anti-goat IgG (1:200; Invitrogen), Alexa Fluor 488 anti-rat IgG (1:200; Invitrogen), Alexa Fluor 488 and 594 anti-mouse IgG (1:200; Invitrogen), and Alexa Fluor 594 anti-rabbit IgG (1:200; Invitrogen). Vectastain Elite ABC system kits were used for IHC (Vector Laboratories).

*BM harvest and transplantation*. BMCs were harvested from donor mice as previously described (13). Briefly, femurs and tibias were isolated and flushed with sterile HBBS (Gibco) with penicillin/streptomycin/fungisone. Cells were washed 2× with sterile HBBS, dissociated with 18-gauge needles, and filtered through 70-μm nylon mesh. For transplantation experiments, $2 \times 10^6$ BMCs from *Rag1$^{-/-}$xEGFPTg* donor mice were injected into the retro-orbital sinus 8–10 hours after irradiation of recipient mice (6 Gy). Antibiotics were added to drinking water for 14 days following the procedure. At the end of each experiment, recipient mice were anesthetized by i.p. injection of Avertin and vasculature was exsanguinated by perfusion of sterile PBS through the left ventricle.

*Flow cytometry and FACS*. Freshly harvested tissues were digested in 1 mg/ml collagenase A for 1–4 hours at 37°C with continuous rotation. Resulting cell suspensions were dispersed with an 18-gauge needle, washed 2 × with Resuspension Buffer (2% heat-inactivated FCS in sterile HBBS), and filtered through 70-μm nylon mesh. Single-cell suspensions were prepared for flow cytometry by suspension in PBS containing 2% FCS and 0.01% NaN3, labeled with appropriate antibodies for 30 minutes at 4°C, acquired on a FACSCanto II (FACSDiva software 5.02; BD Biosciences), and ana-

lyzed using FlowJo software (Tree Star, Inc.). Dead cells were excluded using Live/Dead Fixable Aqua cell stain (Invitrogen). In some cases, samples were blocked with an antibody to CD16/CD32 $F_c\gamma$ III/II receptor (250 ng/$10^6$ cells; BD Pharmingen). Antibodies used for flow cytometry were as follows: PE-cy5–anti-Ly-6A/E/Sca-1 (clone D7; eBioscience), PE–anti-CD117/c-Kit (2B8, eBioscience), APC–Alexa 780–anti-CD45 (30-F11; eBioscience), Pacific blue–anti-CD11b/Mac-1 (M1/70; eBioscience), PE-Cy7–anti-Gr1 (RB6-8C5; eBioscience), Fitc–anti-NK1.1 (NK1.1, NKR-P1C, Ly-55; eBioscience), APC–anti-CD11c (Integrin alpha x, p150/90; eBioscience), APC–anti-VEGFR1/Flt1 (141522; eBioscience), Alexa Fluor 647–goat anti-rabbit; Alexa Fluor 647–goat anti-rat (200 ng/$10^6$ cells; Molecular Probes); and mouse lineage panel kit (BD Biosciences — Pharmingen). FACS antibodies were as follows: PE–anti-Ly-6A/E/Sca-1 (400 ng/$10^6$ cells; clone E13-161.7; BD Biosciences — Pharmingen); APC/PE-anti-CD117/c-Kit (400 ng/$10^6$ cells, clone 2B8; BD Biosciences — Pharmingen).

*RNA preparation, gene expression array, and computational analyses.* BMCs were treated as follows: $Sca1^+cKit^-$ BMCs were isolated by FACS directly into TriZOL reagent (Invitrogen). RNA preparation, amplification, hybridization, and scanning were performed according to standard protocols (66). Gene expression profiling of $Sca1^+cKit^-$ BMCs from mice was performed on Affymetrix MG-430A microarrays. Fibroblasts were treated as follows: triplicate samples of the human fibroblast cell line hMF-2 were cultured in the presence of 1 μg/ml of recombinant human GRN (R&D systems), added daily, for a total duration of 6 days. Total RNA was extracted from fibroblasts using RNA extraction kits according to the manufacturer's instructions (QIAGEN). Gene expression profiling of GRN-treated versus untreated fibroblasts was performed on Affymetrix HG-U133A plus 2 arrays. Arrays were normalized using the Robust Multichip Average (RMA) algorithm (67). To identify differentially expressed genes, we used Smyth's moderated *t* test (68). To test for enrichments of higher- or lower-expressed genes in gene sets, we used the RenderCat program (69), which implements a threshold-free technique with high statistical power based on the Zhang C statistic. As gene sets, we used the Gene Ontology collection (http://www.geneontology.org) and the Applied Biosystems Panther collection (http://www.pantherdb.org). Full data sets are available online: $Sca1^+cKit-$ BMCs, GEO GSE25620; human mammary fibroblasts, GEO GSE25619.

*Cellular image analysis using CellProfiler.* Image analysis and quantification were performed on both immunofluorescence and immunohistological images using the open-source software CellProfiler (http://www.cellprofiler.org) (18, 19). Analysis pipelines were designed as follows: (a) For chromagen-based αSMA immunohistological images, each color image was split into its red, green, and blue component channels. The αSMA-stained area was enhanced for identification by pixel-wise subtracting the green channel from the red channel. These enhanced areas were identified and quantified on the basis of the total pixel area occupied as determined by automatic image thresholding. (b) For αSMA- and DAPI-stained immunofluorescence images, the αSMA-stained region was identified from each image and quantified on the basis of the total pixel area occupied by the αSMA stain as determined by automatic image thresholding. The nuclei were also identified and counted using automatic thresholding and segmentation methods. (c) For αSMA and GRN immunofluorescence images, the analysis was identical to (b) with the addition of a GRN identification module. Both the αSMA- and GRN-stained regions were quantified on the basis of the total pixel area occupied by the respective stains. (d) For chromagen-based GRN immunohistological images, the analysis described in (a) is also applicable for identification of the GRN stain. The area of the GRN-stained region was quantified as a percentage of the total tissue area as identified by the software. All image analysis pipelines used in these studies are available online at the CellProfiler site (http://www.cellprofiler.org/published_pipelines.shtml#Elkabets_2010).

*GRN treatment of human mammary fibroblasts.* Human mammary fibroblasts were isolated from reduction mammoplasties and immortalized by transduction of an hTERT-GFP fusion protein and cultured under standard conditions as described previously (70). Briefly, 2 preparations of such immortalized fibroblast cell lines, termed hMF-1 and hMF-2, were treated with daily doses of 5 ng/ml of recombinant human TGF-β1 (R&D Systems) or 250 ng/ml or 1 μg/ml of recombinant human GRN (R&D Systems) for a duration of 6 days. Immunofluorescence analysis of αSMA expression was performed as previously described using Cy3-conjugated anti-αSMA antibody (Sigma-Aldrich) (70).

*Human tissue specimens and TMA.* Ethical approval for the use of breast cancer specimens for this study was obtained from the Ethics Committee at Lund University (ref no 447-07), whereby written consent was not required and patients were offered the option to opt out. The specimens used in this study were obtained from 144 patients diagnosed with breast cancer at the department of Pathology, Malmö University Hospital (Malmö, Sweden) between 2001 and 2002. The median age at diagnosis was 65 years (range 34–97), and the median follow-up time for disease-specific and overall survival was 78 months. 21% of all patients in this cohort had received adjuvant chemotherapy. All tissue cases were histopathologically reevaluated on slides stained with H&E prior to TMA construction. Representative areas were marked and the TMA was constructed as described previously (71, 72). Cores of 1 mm for 144 individual breast tumors, in duplicates, were used for creating the TMA. Primary antibodies used for GRN staining of TMAs included HPA028747 (1:100; AtlasAntibodies), HPA008763 (1:50; AtlasAntibodies), and CAB019394 (1:600; Strategic Diagnostics). Automated immunohistochemistry (Autostainer 480; Lab Vision) was performed as previously described (73).

*GRN ELISAs.* Murine plasma was collected as described (13). Murine GRN levels were measured by quantitative sandwich assay using anti-GRN primary antibody (#MAB25571 clone 333731; 4 μg/ml) and biotin-conjugated secondary antibody (BAF2557; 1 μg/ml; R&D Systems) according to standard protocols.

*GRN mRNA expression.* RNA was extracted from sorted $Sca1^+cKit^-$ cells by RNeasy Micro Kit (QIAGEN). Reverse transcriptase and preamplification were done by the High Capacity cDNA Reverse Transcription Kit and TaqMan PreAmp (ABI), respectively. Quantitative PCR (qPCR) analysis was assessed by ABI-7300, and GRN expression was calculated relative to 2 housekeeping genes; β-2 microglobulin (B2M) and β-actin (Actb). Probe numbers were as follows: B2M (Mm00437762_m1*); Actb (Mm01205647_g1); and GRN (Mm00433848_m1*).

*Statistics.* For human TMA data, $\chi^2$ and Spearman's correlation tests were used for comparison of protein expression and patient and tumor characteristics. All statistical tests were 2 sided; $P < 0.05\%$ was considered significant. Log-rank test were used for Kaplan-Meier analysis. All statistics were performed using IBM SPSS Statistics 18.0 (SPSS Inc.). Unless otherwise specified, all other data are expressed as mean ± SEM, and data analyzed by Student's *t* test were considered statistically significant if $P < 0.05$.

## Acknowledgments

This work was supported by grants from the David H. Koch Cancer Research Fund and the Alexander and Margaret Stewart Trust Fund (to S.S. McAllister), the Broad Institute and the NIH (R01 GM089652-01 to A.E. Carpenter), the Knut and Alice Wallenberg Research Foundation (to F. Pontén), and the Breast Cancer Research Foundation and National Cancer Institute (CA12515 to R.A. Weinberg). R.A. Weinberg is an American Cancer Society

research professor and a Daniel K. Ludwig Cancer research professor. The authors would like to thank Amanda S. Robinson, Hanna Kuznetsov, Sabine Schneider, and Jennifer Love for technical assistance, and members of the McAllister and Weinberg labs for helpful discussion. We thank Jessica Hughes, Hematology Division, Brigham and Women's Hospital, for help in preparation of the manuscript.

Received for publication May 19, 2010, and accepted in revised form December 1, 2010.

Address correspondence to: Sandra S. McAllister, Harvard Medical School, Brigham and Women's Hospital, 1 Blackfan Circle, Karp 5-214, Boston, Massachusetts 02115, USA. Phone: 617.355.9059; Fax: 617.355.9093; E-mail: smcallister1@partners.org.

1. Schoenberg BS. Multiple primary malignant neoplasms. The Connecticut experience, 1935–1964. *Recent Results Cancer Res*. 1977;58:1–173.
2. Watanabe S, et al. Multiple primary cancers in 5,456 autopsy cases in the National Cancer Center of Japan. *J Natl Cancer Inst*. 1984;72(5):1021–1027.
3. Schaapveld M, et al. Risk of new primary nonbreast cancers after breast cancer treatment: a Dutch population-based study. *J Clin Oncol*. 2008;26(8):1239–1246.
4. Schaapveld M, et al. The impact of adjuvant therapy on contralateral breast cancer risk and the prognostic significance of contralateral breast cancer: a population based study in the Netherlands. *Breast Cancer Res Treat*. 2008;110(1):189–197.
5. Carmichael AR, Bendall S, Lockerbie L, Prescott R, Bates T. The long-term outcome of synchronous bilateral breast cancer is worse than metachronous or unilateral tumours. *Eur J Surg Oncol*. 2002;28(4):388–391.
6. Ruiterkamp J, Ernst MF, van de Poll-Franse LV, Bosscha K, Tjan-Heijnen VC, Voogd AC. Surgical resection of the primary tumour is associated with improved survival in patients with distant metastatic breast cancer at diagnosis. *Eur J Surg Oncol*. 2009;35(11):1146–1151.
7. Ruiterkamp J, Voogd AC, Bosscha K, Tjan-Heijnen VC, Ernst MF. Impact of breast surgery on survival in patients with distant metastases at initial presentation: a systematic review of the literature. *Breast Cancer Res Treat*. 2010;120(1):9–16.
8. McAllister SS, Weinberg RA. Tumor-host interactions: a far-reaching relationship. *J Clin Oncol*. 2010;28(26):4022–4028.
9. McAllister SS, et al. Systemic endocrine instigation of indolent tumor growth requires osteopontin. *Cell*. 2008;133(6):994–1005.
10. Shojaei F, et al. Tumor refractoriness to anti-VEGF treatment is mediated by CD11b+Gr1+ myeloid cells. *Nat Biotechnol*. 2007;25(8):911–920.
11. Ince TA, et al. Transformation of different human breast epithelial cell types leads to distinct tumor phenotypes. *Cancer Cell*. 2007;12(2):160–170.
12. Elenbaas B, et al. Human breast cancer cells generated by oncogenic transformation of primary mammary epithelial cells. *Genes Dev*. 2001;15(1):50–65.
13. Bissell MJ, Radisky D. Putting tumours in context. *Nat Rev Cancer*. 2001;1(1):46–54.
14. Hirschi KK, D'Amore PA. Pericytes in the microvasculature. *Cardiovasc Res*. 1996;32(4):687–698.
15. Song S, Ewald AJ, Stallcup W, Werb Z, Bergers G. PDGFRbeta+ perivascular progenitor cells in tumours regulate pericyte differentiation and vascular survival. *Nat Cell Biol*. 2005;7(9):870–879.
16. Walker RA. The complexities of breast cancer desmoplasia. *Breast Cancer Res*. 2001;3(3):143–145.
17. Kalluri R, Zeisberg M. Fibroblasts in cancer. *Nat Rev Cancer*. 2006;6(5):392–401.
18. Carpenter AE, et al. CellProfiler: image analysis software for identifying and quantifying cell phenotypes. *Genome Biol*. 2006;7(10):R100.
19. Lamprecht MR, Sabatini DM, Carpenter AE. CellProfiler: free, versatile software for automated biological image analysis. *Biotechmiques*. 2007;42(1):71–75.
20. Pazolli E, et al. Senescent stromal-derived osteopontin promotes preneoplastic cell growth. *Cancer Res*. 2009;69(3):1230–1239.
21. Polyak K, Kalluri R. The role of the microenvironment in mammary gland development and cancer. *Cold Spring Harb Perspect Biol*. 2010;2(11):a003244.
22. Ishii G, et al. Bone-marrow-derived myofibroblasts contribute to the cancer-induced stromal reaction. *Biochem Biophys Res Commun*. 2003;309(1):232–240.
23. Radisky DC, Kenny PA, Bissell MJ. Fibrosis and cancer: do myofibroblasts come also from epithelial cells via EMT? *J Cell Biochem*. 2007;101(4):830–839.
24. Pietras K, Pahler J, Bergers G, Hanahan D. Functions of paracrine PDGF signaling in the proangiogenic tumor stroma revealed by pharmacological targeting. *PLoS Med*. 2008;5(1):e19.
25. Randall TD, Weissman IL. Characterization of a population of cells in the bone marrow that phenotypically mimics hematopoietic stem cells: resting stem cells or mystery population? *Stem Cells*. 1998;16(1):38–48.
26. Ortiz M, Wine JW, Lohrey N, Ruscetti FW, Spence SE, Keller JR. Functional characterization of a novel hematopoietic stem cell and its place in the c-Kit maturation pathway in bone marrow cell development. *Immunity*. 1999;10(2):173–182.
27. Kumar R, Fossati V, Israel M, Snoeck HW. Lin- Sca1+kit- bone marrow cells contain early lymphoid-committed precursors that are distinct from common lymphoid progenitors. *J Immunol*. 2008;181(11):7507–7513.
28. Harman BC, Northrup DL, Allman D. Resolution of unique Sca-1highc-Kit- lymphoid-biased progenitors in adult bone marrow. *J Immunol*. 2008; 181(11):7514–7524.
29. Trowbridge JJ, Guezguez B, Moon RT, Bhatia M. Wnt3a activates dormant c-Kit(–) bone marrow-derived cells with short-term multilineage hematopoietic reconstitution capacity. *Stem Cells*. 2010;28(8):1379–1389.
30. Bateman A, Bennett HP. The granulin gene family: from cancer to dementia. *Bioessays*. 2009;31(11):1245–1254.
31. Desmouliere A, Geinoz A, Gabbiani F, Gabbiani G. Transforming growth factor-beta 1 induces alpha-smooth muscle actin expression in granulation tissue myofibroblasts and in quiescent and growing cultured fibroblasts. *J Cell Biol*. 1993;122(1):103–111.
32. Serini G, Gabbiani G. Mechanisms of myofibroblast activity and phenotypic modulation. *Exp Cell Res*. 1999;250(2):273–283.
33. Chang HY, et al. Diversity, topographic differentiation, and positional memory in human fibroblasts. *Proc Natl Acad Sci U S A*. 2002;99(20):12877–12882.
34. Chang HY, et al. Gene expression signature of fibroblast serum response predicts human cancer progression: similarities between tumors and wounds. *PLoS Biol*. 2004;2(2):E7.
35. Sugimoto T, et al. Growth factor-mediated interaction between tumor cells and stromal fibroblasts in an experimental model of human small-cell lung cancer. *Oncol Rep*. 2005;14(4):823–830.
36. Anderberg C, et al. Paracrine signaling by platelet-derived growth factor-CC promotes tumor growth by recruitment of cancer-associated fibroblasts. *Cancer Res*. 2009;69(1):369–378.
37. Erez N, Truitt M, Olson P, Hanahan D. Cancer-associated fibroblasts are activated in incipient neoplasia to orchestrate tumor-promoting inflammation in an NF-kappaB-dependent manner. *Cancer Cell*. 2010;17(2):135–147.
38. Zanocco-Marani T, Bateman A, Romano G, Valentinis B, He ZH, Baserga R. Biological activities and signaling pathways of the granulin/epithelin precursor. *Cancer Res*. 1999;59(20):5331–5340.
39. He Z, Bateman A. Progranulin (granulin-epithelin precursor, PC-cell-derived growth factor, acrogranin) mediates tissue repair and tumorigenesis. *J Mol Med*. 2003;81(10):600–612.
40. Jones MB, et al. The granulin-epithelin precursor/PC-cell-derived growth factor is a growth factor for epithelial ovarian cancer. *Clin Cancer Res*. 2003; 9(1):44–51.
41. Cheung ST, et al. Granulin-epithelin precursor overexpression promotes growth and invasion of hepatocellular carcinoma. *Clin Cancer Res*. 2004; 10(22):7629–7636.
42. Ho JC, et al. Granulin-epithelin precursor as a therapeutic target for hepatocellular carcinoma. *Hepatology*. 2008;47(5):1524–1532.
43. Uhlen M, et al. Towards a knowledge-based human protein atlas. *Nat Biotechnol*. 2010;28(12):1248–1250.
44. Perou CM, et al. Molecular portraits of human breast tumours. *Nature*. 2000;406(6797):747–752.
45. Schneider BP, et al. Triple-negative breast cancer: risk factors to potential targets. *Clin Cancer Res*. 2008;14(24):8010–8018.
46. Kennecke H, et al. Metastatic behavior of breast cancer subtypes. *J Clin Oncol*. 2010;28(20):3271–3277.
47. Van Scott EJ, Reinertson RP. The modulating influence of stromal environment on epithelial cells studied in human autotransplants. *J Invest Dermatol*. 1961;36:109–131.
48. Eyden B, Banerjee SS, Shenjere P, Fisher C. The myofibroblast and its tumours. *J Clin Pathol*. 2009; 62(3):236–249.
49. Mueller MM, Fusenig NE. Friends or foes - bipolar effects of the tumour stroma in cancer. *Nat Rev Cancer*. 2004;4(11):839–849.
50. Korc M. Pancreatic cancer-associated stroma production. *Am J Surg*. 2007;194(4 suppl):S84–S86.
51. Mahadevan D, Von Hoff DD. Tumor-stroma interactions in pancreatic ductal adenocarcinoma. *Mol Cancer Ther*. 2007;6(4):1186–1197.
52. Micke P, Ostman A. Tumour-stroma interaction: cancer-associated fibroblasts as novel targets in anti-cancer therapy? *Lung Cancer*. 2004; 45 suppl 2:S163–S175.
53. Zeisberg EM, Potenta S, Xie L, Zeisberg M, Kalluri R. Discovery of endothelial to mesenchymal transition as a source for carcinoma-associated fibroblasts. *Cancer Res*. 2007;67(21):10123–10128.
54. Direkze NC, et al. Bone marrow contribution to tumor-associated myofibroblasts and fibroblasts. *Cancer Res*. 2004;64(23):8492–8495.
55. Sangai T, et al. Effect of differences in cancer cells and tumor growth sites on recruiting bone marrow-derived endothelial cells and myofibroblasts in cancer-induced stroma. *Int J Cancer*. 2005;115(6):885–892.
56. Bellini A, Mattoli S. The role of the fibrocyte, a bone marrow-derived mesenchymal progenitor, in reactive and reparative fibroses. *Lab Invest*. 2007;87(9):858–870.
57. Worthley DL, et al. Human gastrointestinal neoplasia-associated myofibroblasts can develop from bone marrow-derived cells following allogeneic stem cell transplantation. *Stem Cells*. 2009;27(6):1463–1468.
58. Andreu P, et al. FcRgamma activation regulates

inflammation-associated squamous carcinogenesis. *Cancer Cell*. 2010;17(2):121–134.
59. Li Y, et al. B cells and T cells are critical for the preservation of bone homeostasis and attainment of peak bone mass in vivo. *Blood*. 2007;109(9):3839–3848.
60. Xiao S, Su DM, Manley NR. T cell development from kit-negative progenitors in the Foxn1Delta/Delta mutant thymus. *J Immunol*. 2008;180(2):914–921.
61. Serrero G, Ioffe OB. Expression of PC-cell-derived growth factor in benign and malignant human breast epithelium. *Hum Pathol*. 2003;34(11):1148–1154.
62. Jones MB, Spooner M, Kohn EC. The granulin-epithelin precursor: a putative new growth factor for ovarian cancer. *Gynecol Oncol*. 2003;88(1 pt 2):S136–S139.
63. Davidson B, et al. Granulin-epithelin precursor is a novel prognostic marker in epithelial ovarian carcinoma. *Cancer*. 2004;100(10):2139–2147.
64. Pan CX, et al. PC cell-derived growth factor expression in prostatic intraepithelial neoplasia and prostatic adenocarcinoma. *Clin Cancer Res*. 2004; 10(4):1333–1337.
65. Ethier SP, Mahacek ML, Gullick WJ, Frank TS, Weber BL. Differential isolation of normal luminal mammary epithelial cells and breast cancer cells from primary and metastatic sites using selective media. *Cancer Res*. 1993;53(3):627–635.
66. Ebert BL, et al. An erythroid differentiation signature predicts response to lenalidomide in myelodysplastic syndrome. *PLoS Med*. 2008;5(2):e35.
67. Irizarry RA, et al. Exploration, normalization, and summaries of high density oligonucleotide array probe level data. *Biostatistics*. 2003;4(2):249–264.
68. Smyth GK. Linear models and empirical bayes methods for assessing differential expression in microarray experiments. *Stat Appl Genet Mol Biol*. 2004;3:Article3.
69. Nilsson B, Hakansson P, Johansson M, Nelander S, Fioretos T. Threshold-free high-power methods for the ontological analysis of genome-wide gene-expression studies. *Genome Biol*. 2007;8(5):R74.
70. Orimo A, et al. Stromal fibroblasts present in invasive human breast carcinomas promote tumor growth and angiogenesis through elevated SDF-1/CXCL12 secretion. *Cell*. 2005;121(3):335–348.
71. Kononen J, et al. Tissue microarrays for high-throughput molecular profiling of tumor specimens. *Nat Med*. 1998;4(7):844–847.
72. Kallioniemi OP, Wagner U, Kononen J, Sauter G. Tissue microarray technology for high-throughput molecular profiling of cancer. *Hum Mol Genet*. 2001;10(7):657–662.
73. Nilsson P, et al. Towards a human proteome atlas: high-throughput generation of mono-specific antibodies for tissue profiling. *Proteomics*. 2005;5(17):4327–4337.